



LAWRENCE  
LIVERMORE  
NATIONAL  
LABORATORY

# BINARY QUASARS IN THE SLOAN DIGITAL SKY SURVEY: EVIDENCE FOR EXCESS CLUSTERING ON SMALL SCALES

J. F. Hennawi, M. A. Strauss, M. Oguri, N. Inada, G. T. Richards, B. Pindor, D. P. Schneider, R. H. Becker, M. D. Gregg, P. B. Hall, D. E. Johnston, X. Fan, S. Burles, D. J. Schlegel, J. E. Gunn, R. Lupton, N. A. Bahcall, R. J. Brunner, J. Brinkman

January 31, 2006

Astronomical Journal

## **Disclaimer**

---

This document was prepared as an account of work sponsored by an agency of the United States Government. Neither the United States Government nor the University of California nor any of their employees, makes any warranty, express or implied, or assumes any legal liability or responsibility for the accuracy, completeness, or usefulness of any information, apparatus, product, or process disclosed, or represents that its use would not infringe privately owned rights. Reference herein to any specific commercial product, process, or service by trade name, trademark, manufacturer, or otherwise, does not necessarily constitute or imply its endorsement, recommendation, or favoring by the United States Government or the University of California. The views and opinions of authors expressed herein do not necessarily state or reflect those of the United States Government or the University of California, and shall not be used for advertising or product endorsement purposes.

## BINARY QUASARS IN THE SLOAN DIGITAL SKY SURVEY: EVIDENCE FOR EXCESS CLUSTERING ON SMALL SCALES

JOSEPH F. HENNAWI,<sup>1,2,3</sup> MICHAEL A. STRAUSS,<sup>3</sup> MASAMUNE OGURI,<sup>3,4</sup> NAOHISA INADA,<sup>5</sup> GORDON T. RICHARDS,<sup>3</sup> BARTOSZ PINDOR,<sup>6,7</sup> DONALD P. SCHNEIDER,<sup>8</sup> ROBERT H. BECKER,<sup>9,10</sup> MICHAEL D. GREGG,<sup>9,10</sup> PATRICK B. HALL,<sup>11</sup> DAVID E. JOHNSTON,<sup>3</sup> XIAOHUI FAN,<sup>12</sup> SCOTT BURLES,<sup>13</sup> DAVID J. SCHLEGEL,<sup>14</sup> JAMES E. GUNN,<sup>3</sup> ROBERT LUPTON,<sup>3</sup> NETA A. BAHCALL,<sup>3</sup> ROBERT J. BRUNNER,<sup>15</sup> JON BRINKMAN<sup>16</sup>

*Draft version January 30, 2006*

### ABSTRACT

We present a sample of 218 new quasar pairs with proper transverse separations  $R_{\text{prop}} < 1 h^{-1}$  Mpc over the redshift range  $0.5 < z < 3.0$ , discovered from an extensive follow up campaign to find companions around the Sloan Digital Sky Survey and 2dF Quasar Redshift Survey quasars. This sample includes 26 new binary quasars with separations  $R_{\text{prop}} < 50 h^{-1}$  kpc ( $\theta < 10''$ ), more than doubling the number of such systems known. We define a statistical sample of binaries selected with homogeneous criteria and compute its selection function, taking into account sources of incompleteness. The first measurement of the quasar correlation function on scales  $10 h^{-1}$  kpc  $< R_{\text{prop}} < 400 h^{-1}$  kpc is presented. For  $R_{\text{prop}} \lesssim 40 h^{-1}$  kpc, we detect an order of magnitude excess clustering over the expectation from the large scale ( $R_{\text{prop}} \gtrsim 3 h^{-1}$  Mpc) quasar correlation function, extrapolated down as a power law to the separations probed by our binaries. The excess grows to  $\sim 30$  at  $R_{\text{prop}} \sim 10 h^{-1}$  kpc, and provides compelling evidence that the quasar autocorrelation function gets progressively steeper on sub-Mpc scales. This small scale excess can likely be attributed to dissipative interaction events which trigger quasar activity in rich environments. Recent small scale measurements of galaxy clustering and quasar-galaxy clustering are reviewed and discussed in relation to our measurement of small scale quasar clustering.

*Subject headings:* general – quasars: general – cosmology: general – surveys: observations – large-scale structure of the Universe

### 1. INTRODUCTION

A fundamental problem for cosmologists is to understand how quasars are embedded in the galaxy formation hierarchy and to relate them to the gravitational evolu-

tion of the structure of the underlying dark matter. In the current paradigm, every massive galaxy is thought to have undergone a luminous quasar phase, and quasars at high redshift are the progenitors of the local dormant supermassive black hole population found in the centers of nearly all nearby bulge-dominated galaxies (e.g. Small & Blandford 1992; Yu & Tremaine 2002). This fundamental connection is supported by the tight correlations between the masses of central black holes and the velocity dispersions of their old stellar populations (Magorrian et al. 1998; Ferrarese & Merritt 2000; Gebhardt et al. 2000; Tremaine et al. 2002) and by comparing the number density of black holes in the local Universe to the luminosity density produced by quasars at high redshift (Small & Blandford 1992; Yu & Tremaine 2002).

Quasars are likely to reside in massive hosts (Turner 1991) and it has been suggested that they occupy the rarest peaks in the initial Gaussian density fluctuation distribution (Efstathiou & Rees 1988; Cole & Kaiser 1989; Nusser & Silk 1993; Djorgovski et al. 1999; Djorgovski 1999; Djorgovski et al. 2003; Stiavelli et al. 2005). It is also thought that quasar activity is triggered by the frequent mergers which are a generic consequence of bottom up structure formation models (Bahcall et al. 1997; Carlberg 1990; Haehnelt & Rees 1993; Wyithe & Loeb 2002b). Both of these hypothesis imply that quasars should be highly biased tracers of the dark matter distribution: rare peaks in the density field are intrinsically strongly clustered (Kaiser 1984) and the frequency of mergers is higher in dense environments (Lacey & Cole 1993). Measurements of quasar clustering can thus teach us about the environments of quasars as well as give clues

<sup>1</sup> Hubble Fellow

<sup>2</sup> Department of Astronomy, University of California at Berkeley, 601 Campbell Hall, Berkeley, CA 94720-3411.

<sup>3</sup> Princeton University Observatory, Peyton Hall, Princeton, NJ 08544.

<sup>4</sup> Department of Physics, University of Tokyo, Hongo 7-3-1, Bunkyo-ku, Tokyo 113-0033, Japan.

<sup>5</sup> Institute of Astronomy, University of Tokyo, 2-21-1 Osawa, Mitaka, Tokyo 181-8588, Japan.

<sup>6</sup> Department of Astronomy, University of Toronto, 60 St George Street, Toronto M5S3H8, Canada

<sup>7</sup> CFHT Legacy Survey Postdoctoral Fellow

<sup>8</sup> Department of Astronomy and Astrophysics, Pennsylvania State University, 525 Davey Laboratory, University Park, PA 16802.

<sup>9</sup> Department of Physics, University of California at Davis, 1 Shields Avenue, Davis, CA 95616.

<sup>10</sup> Institute of Geophysics and Planetary Physics, Lawrence Livermore National Laboratory, L-413, 7000 East Avenue, Livermore, CA 94550.

<sup>11</sup> Department of Physics & Astronomy, York University, 4700 Keele St., Toronto, ON M3J 1P3, Canada.

<sup>12</sup> Steward Observatory, University of Arizona, 933 North Cherry Avenue, Tucson, AZ 85721

<sup>13</sup> Physics Department, Massachusetts Institute of Technology, 77 Massachusetts Avenue, Cambridge, MA 02139.

<sup>14</sup> Lawrence Berkeley National Laboratory, One Cyclotron Road, Mailstop 50R232, Berkeley, CA, 94720, USA.

<sup>15</sup> Department of Astronomy and National Center for Supercomputer Applications, University of Illinois, 1002 West Green Street, Urbana, IL 61801.

<sup>16</sup> Apache Point Observatory, P. O. Box 59, Sunspot, NM88349-0059.

to the dynamical processes which trigger quasar activity. Furthermore, a comparison of quasar clustering with the quasar luminosity function can be used to constrain the mean quasar lifetime (Haiman & Hui 2001; Martini & Weinberg 2001) as well as the relationship between the mass of central black holes and the circular velocities of their host dark halos (Wyithe & Loeb 2004).

There have been many attempts to measure quasar clustering, beginning with the pioneering work of Osmer (1981). Shaver (1984) first detected quasar clustering using a clever technique to measure correlations from inhomogeneous catalogs and discovered that quasars were clustered similar to galaxies in the local universe, a result later confirmed by Kruszewski (1988). Most recently, Croom et al. (2001), Porciani, Magliocchetti, & Norberg (2004) (henceforth PMN), and Croom et al. (2005) measured the clustering of quasars in the redshift range  $z = 0.3 - 2.2$  from the  $\sim 15,000$  quasars in the Two Degree Field Quasar Survey (2QZ) (Croom et al. 2004b). They both find good agreement with a power law correlation function  $\xi(r) = (r/r_0)^{-\gamma}$  on scales  $r = 1 - 35 h^{-1}$  Mpc, with correlation length  $r_0 \sim 5 h^{-1}$  Mpc (comoving) and slope  $\gamma \sim 1.5$ , with only a weak dependence on redshift and luminosity (Croom et al. 2002). This agrees with previous measurements (Iovino & Shaver 1988; Andreani & Cristiani 1992; Mo & Fang 1993; Shanks & Boyle 1994; Croom & Shanks 1996) and is similar to the clustering of nearby galaxies.

At redshift  $z > 2.5$ , quasars are rarer and thus quasar clustering has been much more difficult to measure. However the mere existence of a few high redshift quasar pairs provides circumstantial evidence that quasars may have been much more highly clustered in the past. In the Palomar Transit Grism Survey of Schneider et al. (1994), three quasar pairs with  $z \gtrsim 3$  and comoving separations  $5 - 10 h^{-1}$  Mpc were found in a complete sample of 90 quasars covering  $61.5 \text{ deg}^2$ . Analysis of clustering in this high redshift sample by Kundic (1997) and Stephens et al. (1997) detected a statistically significant clustering signal, dominated by the three pairs, which implied a comoving correlation length  $r_0 \sim 50 h^{-1}$  Mpc. This is much larger than the correlation length of present day galaxies or  $z \sim 1.5$  quasars. The only sub-arcminute high redshift quasar pair known is a  $33''$  pair of quasars at  $z = 4.25$  discovered serendipitously by Schneider et al. (2000). Based on the discovery of this one object with proper transverse separation of  $162 h^{-1}$  kpc, they estimated the correlation length could be as large as  $\sim 30 h^{-1}$  Mpc. Djorgovski et al. (2003) discovered a companion at  $z = 5.02$  separated by  $196''$  from the high redshift quasar at  $z = 4.96$  discovered by Fan et al. (1999), corresponding to a proper transverse separation of  $896 h^{-1}$  kpc. This is the highest redshift pair of quasars known.

Even in the large quasar sample studied by Croom et al. (2001), PMN, and Croom et al. (2005), the smallest scale at which the correlation function can be measured is  $\sim 1 h^{-1}$  Mpc. The reason for this is twofold. First, close quasar pairs with angular separations  $\lesssim 60''$ , corresponding to  $\sim 1 h^{-1}$  Mpc at  $z \sim 1.5$ , are extremely rare, simply because at small separations, the correlation function does not increase as fast as the volume decreases. Second, because of the finite size of the optical fibers of the 2dF multi-object spectrograph, only one quasar in a close pair with separation  $< 30''$  can be observed. This

limitation, referred to as a *fiber collision*, is also a problem for the Sloan Digital Sky Survey (York et al. 2000, SDSS), for which this angular scale is  $55''$  (Blanton et al. 2003).

A significant motivation for studying small scale quasar clustering, is the existence of controversial population of quasar pairs discovered in the search for gravitationally lensed quasars (Kochanek, Falco, & Muñoz 1999; Mortlock, Webster, & Francis 1999). These close pairs have similar optical spectra, small velocity differences, and typically have separations in the range  $2'' \lesssim \Delta\theta \lesssim 10''$  characteristic of group or cluster scale lenses. However, deep imaging shows no identifiable lenses in the foreground. Although a handful of wide separation ( $\Delta\theta > 3''$ ) gravitational lenses have been discovered (Walsh, Carswell, & Weymann 1979), especially recently in the SDSS (Inada et al. 2003; Oguri et al. 2004, 2005), the expected number of quasars lensed by groups and clusters is too small to account for all of the controversial pairs (Oguri & Keeton 2004; Hennawi et al. 2005). The poster child example is Q 2345+007 (Weedman et al. 1982), the famous pair of  $z = 2.16$  quasars with  $7.1''$  separation. Although a plethora of papers can be found in the literature arguing for (Weedman et al. 1982; Turner et al. 1982; Steidel & Sargent 1991; Bonnet et al. 1993; Fischer et al. 1994; Pello et al. 1996; Small et al. 1997), or against (Phinney & Blandford 1986; Djorgovski 1991; Schneider 1993; Kochanek, Falco, & Muñoz 1999; Mortlock, Webster, & Francis 1999; Green et al. 2002) the lensing hypothesis for this system, the most compelling argument is based on the recent Chandra observations of Green et al. (2002) who failed to detect diffuse X-ray emission associated with the potential lens.

This population has thus led to much speculation about exotic mass concentrations which could be responsible for the apparent multiple imaging. It has been suggested that the lenses in these systems are ‘dark’ galaxies or galaxy clusters (Subramanian, Rees, & Chitre 1987; Duncan 1991; Hawkins et al. 1997; Malhotra et al. 1997; Peng et al. 1999; Koopmans et al. 2000), that they could be lensed by free floating  $\sim 10^{14} M_\odot$  black holes (Turner 1991), or that they might be instances of gravitational lensing by cosmic strings (Vilenkin 1984; Paczynski 1986; Hogan & Narayan 1984).

A much more plausible explanation is that these controversial pairs are binaries rather than lenses (Phinney & Blandford 1986; Djorgovski 1991; Schneider 1993; Kochanek, Falco, & Muñoz 1999; Mortlock, Webster, & Francis 1999) and hence just a manifestation of quasar clustering on small scales. Djorgovski (1991) first pointed out that this interpretation implies a factor of  $\sim 100$  more binary quasars over what is naively expected from extrapolating the quasar correlation function power law down to comoving scales  $\lesssim 100 h^{-1}$  kpc, and he proposed that this was due to the enhancement of quasar activity during merger events. Based on two close pairs found in the LBQS survey, Hewett et al. (1998) similarly claimed an excess of  $\sim 100$  over the expectation from quasar clustering. Kochanek, Falco, & Muñoz (1999) compared the optical and radio properties of the controversial quasar pairs, and argued that they were all binary quasars, and similarly claimed that the excess binaries could be explained in a merger scenario.

The study of binary quasars and small scale quasar

clustering has been hindered by the small number of known examples and the heterogeneous mix of detection methods. In this paper we conduct a systematic search for binary quasars in the SDSS and 2QZ quasar samples. We present a sample of 218 new binary quasars with proper transverse separations  $R_{\text{prop}} < 1 h^{-1}$  Mpc, 24 of which have angular separations  $\lesssim 10''$  corresponding to transverse proper separations  $R_{\text{prop}} \lesssim 50 h^{-1}$  kpc, more than doubling the number of such systems known. A sub-sample of pairs selected with well defined criteria is constructed and we quantify its selection function. Based on this sample, we present the first measurement of the correlation function of quasars on the small scales  $10 h^{-1}$  kpc  $\lesssim R_{\text{prop}} \lesssim 1 h^{-1}$  Mpc. We detect excess small scale clustering compared to the expectation from an extrapolation of the larger scale two point correlation function power law slope.

The outline of this paper is as follows. In §3, we discuss color-selection criteria used to find binary quasars and describe the follow-up observations required to confirm quasar pair candidates in §4. Our binary quasar sample is presented in §5. We show that the number of binary quasars discovered thus far in the SDSS imply an excess of small scale quasar clustering in §6 and we compare this result to small scale galaxy and quasar-galaxy clustering in §7. We summarize and conclude in §8. In the Appendix, we present tables summarizing the results of all of our follow-up observations, as well as a catalog of projected quasar pairs from the SDSS.

Throughout this paper we use the best fit WMAP (only) cosmological model of Spergel et al. (2003), with  $\Omega_m = 0.270$ ,  $\Omega_\Lambda = 0.73$ ,  $h = 0.72$ . Because both proper and comoving distances are used, we will always indicate the former as  $R_{\text{prop}}$ . It is helpful to remember that in the chosen cosmology, for a typical quasar redshift of  $z = 1.5$ , an angular separation of  $\Delta\theta = 1''$  corresponds to a proper (comoving) transverse separation of  $R_{\text{prop}} = 6 h^{-1}$  kpc ( $R = 15 h^{-1}$  kpc), and a velocity difference of  $1000 \text{ km s}^{-1}$  at this redshift corresponds to a proper radial redshift space distance of  $s_{\text{prop}} = 4.4 h^{-1}$  Mpc (comoving  $s = 11 h^{-1}$  Mpc).

## 2. QUASAR SAMPLES

In this section we present a variety of techniques used to select quasar pair candidates. First, we describe the quasar catalogs which served as the parent samples for our quasar pair search. Then we introduce a statistic which quantifies the color similarity of two quasars. Finally, we discuss each selection method in detail and describe our follow-up observations.

### 2.1. The SDSS Spectroscopic Quasar Sample

The Sloan Digital Sky Survey uses a dedicated 2.5m telescope and a large format CCD camera (Gunn et al. 1998) at the Apache Point Observatory in New Mexico to obtain images in five broad bands ( $u$ ,  $g$ ,  $r$ ,  $i$  and  $z$ , centered at 3551, 4686, 6166, 7480 and 8932 Å, respectively; Fukugita et al. 1996; Stoughton et al. 2002) of high Galactic latitude sky in the Northern Galactic Cap. The imaging data are processed by the astrometric pipeline (Pier et al. 2003) and photometric pipeline (Lupton et al. 2001), and are photometrically calibrated to a standard star network (Smith et al. 2002; Hogg et al. 2001). Ad-

ditional details on the SDSS data products can be found in Abazajian et al. (2003, 2004, 2005).

Based on this imaging data, spectroscopic targets chosen by various selection algorithms (i.e. quasars, galaxies, stars, serendipity) are observed with two double spectrographs producing spectra covering 3800–9200 Å with a spectral resolution ranging from 1800 to 2100. Details of the spectroscopic observations can be found in York et al. (2000), Castander et al. (2001), and Stoughton et al. (2002). A discussion of quasar target selection can be found in Richards et al. (2002a). The Third Data Release Quasar Catalog contains 46,420 quasars (Schneider et al. 2005). Here, we use a larger sample of quasars, as we include non-public data: our parent sample includes 67,385 quasars with  $z > 0.3$ , of which 52,279 quasars lie in the redshift range  $0.7 < z < 3.0$ . Note also that we have used the Princeton/MIT spectroscopic reductions<sup>17</sup> which differ slightly from the official SDSS data release.

Most quasar candidates are selected based on their location in multidimensional SDSS color-space. All magnitudes are reddening corrected following the prescription in Schlegel, Finkbeiner, & Davis (1998). Objects with colors that place them outside of the stellar locus which do not inhabit specific “exclusion” regions (e.g., places dominated by white dwarfs, A stars, and M star-white dwarf pairs) are identified as primary quasar candidates. An  $i$  magnitude limit of 19.1 is imposed for candidates whose colors indicate a probable redshift of less than  $\approx 3$ ; high-redshift candidates are accepted if  $i < 20.2$ . Over 90% of SDSS-selected quasars follow a remarkably tight color-redshift relation in the SDSS color-system (Richards et al. 2001a). In addition to the multi-color selection, unresolved objects brighter than  $i = 19.1$  that lie within  $1.5''$  of a FIRST radio source (Becker, White, & Helfand 1995) are also identified as primary quasar candidates.

Supplementing the primary quasar sample described above are quasars targeted by other SDSS target selection packages: Galaxy (the SDSS main and extended galaxy samples Eisenstein et al. 2001; Strauss et al. 2002), X-ray (objects near the position of a ROSAT All-Sky Survey source, Anderson et al. 2003), Star (point source with unusual color), or Serendipity (unusual color or FIRST matches). No attempt at completeness is made for the last three categories; objects selected by these algorithms are observed if a given spectroscopic plate has fibers remaining after all of the high-priority classes (galaxies, quasars, and sky and spectrophotometric calibrations) in the field have been assigned fibers (see Blanton et al. 2003). Most of the quasars that fall below the magnitude limits of the quasar survey were selected by the serendipity algorithm.

As we described in the introduction, the SDSS spectroscopic survey selects *against* close pairs of quasars because of fiber collisions. The finite size of optical fibers implies only one quasar in a pair with separation  $< 55''$  can receive a fiber. Follow-up spectroscopy is thus required to discover quasar pairs. An exception to this rule exists for a fraction ( $\sim 30\%$ ) of the area of the spectroscopic survey covered by overlapping plates. For these plates the same area of sky was observed spectroscopically on more than one occasion so that there is no fiber

<sup>17</sup> Available at <http://spectro.princeton.edu>

collision limitation.

### 2.2. The SDSS Faint Photometric Quasar Sample

Richards et al. (2004) have demonstrated that faint ( $i \lesssim 21$ ) photometric samples of quasars can be constructed from the SDSS photometry, by separating quasars from stars using knowledge of their relative densities in color space. Each member of this catalog is assigned a probability of being a quasar, a photometric redshift, and a probability that the photometric redshift is correct (see Richards et al. 2004 for details). We searched for (and found) quasar pairs in a photometric sample of 273,287 quasar *candidates*. Note that the faint photometric quasar used here is based on the larger SDSS Data Release 3 area (DR3; Abazajian et al. 2005), whereas that published in (Richards et al. 2004) covers the smaller SDSS DR1 area (Abazajian et al. 2003).

### 2.3. The SDSS+2QZ Quasar Sample

The 2dF Quasar Redshift Survey (2QZ) is a homogeneous spectroscopic catalog of 44,576 stellar objects with  $18.25 \leq b_J \leq 20.85$  (Croom et al. 2004b). Of these, 23,338 are quasars spanning the redshift range  $0.3 \lesssim z \lesssim 2.9$ . Selection of quasar candidates is based on broad band colors ( $ub_{JR}$ ) from automated plate measurements of the United Kingdom Schmidt Telescope photographic plates. Spectroscopic observations were carried out with the 2dF instrument, which is a multi-object spectrograph at the Anglo-Australian Telescope. The 2QZ covers a total area of 721.6 deg<sup>2</sup> arranged in two  $75^\circ \times 5^\circ$  strips across the South Galactic Cap (SGP strip), centered on  $\delta = -30^\circ$ , and North Galactic Cap (NGP strip, or equatorial strip), centered at  $\delta = 0^\circ$ . The NGP overlaps the SDSS footprint, corresponding to roughly half of the 2QZ area.

By combining the SDSS quasar catalog with 2QZ quasars in the NGP which have matching SDSS photometry, we arrive at a combined sample of 75,579 quasars with  $z > 0.3$ , of which 67,385 are from the SDSS and 8194 from the 2QZ. For the clustering analysis in § 6 we will restrict attention to the redshift range  $0.7 < z < 3.0$ , for which we define a combined SDSS/2QZ sample of 59,608 quasars, of which 52,279 are from the SDSS and 6879 are from the 2QZ.

## 3. QUASAR PAIR SELECTION

Several different techniques are used to find binary quasars. For small separation pairs,  $\Delta\theta \leq 3''$ , characteristic of the majority of gravitational lenses, binary quasars were discovered in the SDSS search for gravitationally lensed quasars (e.g., Oguri et al. 2005). For wider separations, both components are resolved and we can exploit the precise digital photometry of the SDSS to color select quasar pair candidates. Finally, quasar pairs can be found directly from the spectroscopy: the SDSS contains a fair number of overlapping spectroscopic plates for which fiber collision does not limit the pair separation and quasar pairs can be found by searching the SDSS+2QZ quasar catalog over regions where the survey areas overlap.

### 3.1. Lens Selection

For small separation pairs  $\Delta\theta \leq 3''$ , the two images are unresolved or marginally resolved, as the SDSS imaging

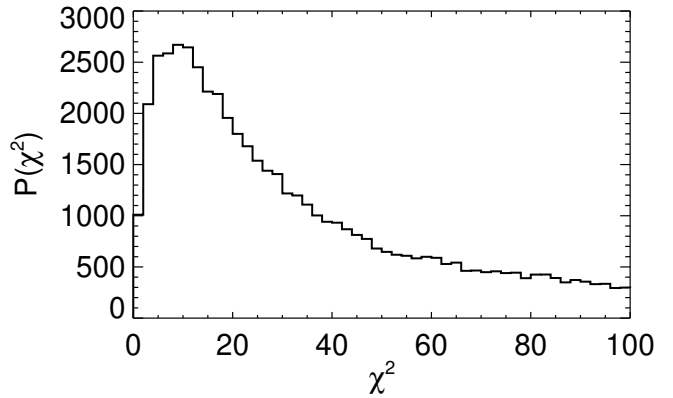


FIG. 1.— Distribution of the  $\chi^2$  statistic for the 64621 unique pair combinations of 359 quasars in the SDSS sample in the redshift interval  $2.4 < z < 2.45$ . The median value of this distribution is 33.1, so that a quasar pair survey which aims to achieve 50% completeness in this redshift interval would have to observe all quasar pair candidates with  $\chi^2 < 33.1$ .

has a median seeing of  $1.4''$ . Candidates are selected by fitting a multi-component PSF model to atlas images of each of the SDSS quasars as described in Pindor et al. (2003) and Inada et al. (2003). We restricted attention to candidates in the redshift range  $0.7 < z < 3.0$ . Quasars with  $z < 0.7$  are unlikely to be gravitational lenses, and the PSF fitting is complicated by the presence of resolved host galaxy emission. The SDSS is biased against gravitational lenses with  $z > 3.0$  because the target selection algorithm for high- $z$  quasars does not target objects classified as extended by the photometric pipeline, and most candidate lenses and binaries appear extended. See the discussion in Pindor et al. (2003) for more details. The number of quasars in this redshift range searched with our lens algorithm was 39,142, which makes up the parent sample of our lens search. This is a subset of the total number (52,279) of SDSS quasars in this range, as the lens algorithm was run on a sample of quasars defined at an earlier date. We refer to objects selected by this algorithm as the ‘lens’ sample.

Follow up observations are required to confirm that the companion object is indeed a quasar at the same redshift. The limiting magnitude for the companion objects is  $i < 21.0$  (here and throughout we always quote reddening corrected asinh magnitudes (Lupton et al. 1999)), as fainter objects are too difficult to observe from the 3.5m telescope at Apache Point Observatory (APO), where most of the follow-up observations were conducted, even in the best conditions (see § 4).

### 3.2. $\chi^2$ Color Selection

Although quasars have a wide range of luminosities, the majority have similar optical/ultraviolet spectral energy distributions. (Richards et al. 2001a) demonstrated that most quasars follow a relatively tight color-redshift relation in the SDSS filter system; a property which has been exploited to calculate photometric redshifts of quasars (Richards et al. 2001b; Budavári et al. 2001; Weinstein et al. 2004). It is thus possible to efficiently select pairs of quasars at the same redshift by searching for

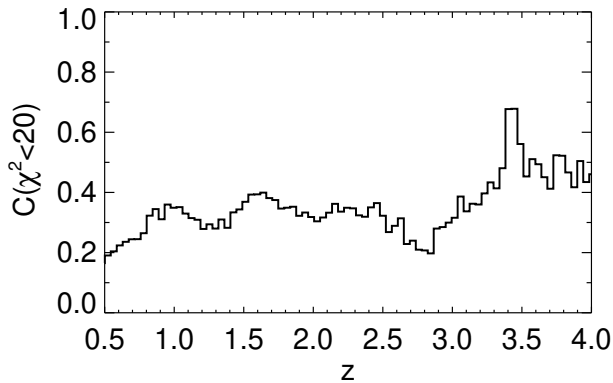


FIG. 2.— Completeness of  $\chi^2$  statistic as a function of redshift for a survey which observes all quasar pair candidates with  $\chi^2 < 20$ . Dispersion in the color-redshift relation of quasars (Richards et al. 2001a) gives rise to a broad distribution of  $\chi^2$  for pairs of quasars at the same redshift (see Figure 1). Restricting the observations of pair candidates to those with  $\chi^2 < 20$  results in  $\sim 35\%$  completeness in the redshift range  $0.70 < z < 3.0$ .

pairs of objects with similar, quasar-like colors.

To this end, we define a statistic that quantifies the likelihood that two astronomical objects have the same color. Recall that a color  $u - g$ , is a statement about flux ratios,  $f^u/f^g$ . Thus if two objects have the same color, then their fluxes should be proportional. Given the fluxes  $f_1^m$  of the first, we can ask whether the fluxes of the second are consistent with the proportionality

$$f_2^m = A f_1^m, \quad (1)$$

where  $f^m$  is a five dimensional vector of fluxes (one for each SDSS band),  $m$  designates the filter, and this relationship holds with the same proportionality constant  $A$  in all bands.

The maximum likelihood value of the parameter  $A$ , given the fluxes of both objects, can be determined by minimizing the  $\chi^2$

$$\chi^2(A) = \sum_{\text{ugriz}} \frac{(f_2^m - A f_1^m)^2}{[\sigma_2^m]^2 + A^2 [\sigma_1^m]^2}, \quad (2)$$

where we have dropped a term corresponding to the normalization of the likelihood because of its slow variation with the parameter  $A$ . The  $\sigma^m$  are the photometric measurement errors, but do not include the intrinsic scatter about the mean color-redshift relation (see discussion below). We thus arrive at the implicit equation for  $A$

$$A = \frac{\sum_{\text{ugriz}} \frac{f_2^m f_1^m}{[\sigma_2^m]^2 + A^2 [\sigma_1^m]^2}}{\sum_{\text{ugriz}} \frac{[f_2^m]^2}{[\sigma_2^m]^2 + A^2 [\sigma_1^m]^2}}, \quad (3)$$

which can be solved in a few iterations. This value is inserted into eqn. (2), reducing the number of degrees of freedom in the  $\chi^2$  to four, i.e. the number of independent colors one could have formed from the five magnitudes.

If the fluxes of the two objects are proportional and if the photometric errors are distributed normally, this statistic follows the chi-squared distribution with four degrees of freedom, and the typical value will be  $\chi^2 \sim 4$ . However the colors of two quasars at the same redshift,

although similar, will in general not be exactly proportional. Fluctuations about the median color-redshift relation of quasars (Richards et al. 2001a) will result in an additional source of ‘dispersion’ in our color similarity statistic. This leads to a much broader distribution of  $\chi^2$  than expected from Gaussian statistical errors. Figure 1 shows the distribution of  $\chi^2$  for the 64621 unique pair combinations of 359 quasars in the redshift interval  $2.4 < z < 2.45$ . The median value of this distribution is 33.1, so that a quasar pair survey which aims to achieve 50% completeness in this redshift interval would have to observe all quasar pair candidates with  $\chi^2 < 33.1$ . Also notice that a long tail in this distribution extends even beyond  $\chi^2 \sim 100$  because of outliers from the median color-redshift relation of quasars (Richards et al. 2001a), caused by broad absorption line features or reddening (Richards et al. 2003; Hopkins et al. 2004).

Our survey for close pairs of quasars thus involves a tradeoff between completeness and efficiency, since tolerating larger values of  $\chi^2$  will increase the number of false pair candidates. Our follow up observations targeted quasar pair candidates with  $\chi^2 < 20$ . This threshold implies a certain level of completeness for our survey, which varies redshift, as the dispersion in the color-redshift relation of quasars depends on redshift (Richards et al. 2001a). We quantify this incompleteness by dividing the SDSS quasar sample into redshift bins of  $\delta z = 0.043$ , and computing the fraction of all the unique combinations of pairs in each bin with  $\chi^2 < 20$ . Figure 2 shows the completeness of our quasar pair survey as a function of redshift. For the redshift range  $0.70 < z < 3.0$ , where most of our binary quasars lie, the  $\chi^2 < 20$  cut results in  $\sim 35\%$  completeness.

Finally, note that the statistic defined by eqn. (2) uses an isotropic ‘metric’ in color-space. This would not be the case had we included the variance of the color-redshift relation  $\sigma^m(z)$  in our errors  $\sigma_{\text{total}}^m$ , similar to the procedure used by Richards et al. (2001b); Weinstein et al. (2004) to determine photometric redshifts of quasars. In retrospect, this would be a more suitable procedure for finding binary quasars. However, we were also conducting a search for wide separation gravitational lenses, and for lenses there is no color-redshift scatter (after all, it is the same quasar observed twice!).

We applied our color similarity statistic to all objects within the annulus  $3'' < \Delta\theta < 60''$  around the 59,608 quasars ( $0.7 < z < 3.0$ ) in the combined SDSS+2QZ catalog. We refer to the binaries selected by searching around the SDSS+2QZ quasars as members of our ‘ $\chi^2$ ’ sample. To be considered for follow up observations, a quasar pair had to meet the following criteria

$$\begin{aligned} \chi^2 &< 20.0 \\ 0.70 &< z < 3.0 \\ i &< 21.0 \\ \sigma_i &< 0.2. \end{aligned} \quad (4)$$

The minimum redshift was imposed because of our desire to find wide separation gravitational lenses (Inada et al. 2003; Oguri et al. 2004). The  $\sigma_i < 0.2$  requirement gets rid of objects with very large photometric errors due to problems with deblending or very poor image quality. In addition, we required that the companion objects be

TABLE 1  
PREVIOUSLY KNOWN BINARY QUASARS IN THE SDSS FOOTPRINT

Name	$z$	$\Delta\theta$	$R_{\text{prop}}$	$ \Delta v $	$i_1$	$i_2$	$\chi^2$	Sample	Notes
SDSSJ 1120+6711	1.49	1.5	9.0	<100	18.49	19.57	–	lens	1
Q 1120+0195	1.47	6.5	39.6	630	15.61	20.26	20.6	–	2
HS 1216+5032	1.46	9.1	55.1	50	16.76	18.31	534.1	overlap	3
Q 1343+2650	2.03	9.2	55.4	200	19.14	19.97	113.7	–	4
LBQS 1429–008	2.08	5.1	30.8	260	17.40	20.74	4.3	$\chi^2$	5
2QZ 1435+0008	2.38	33.2	194.8	760	19.90	20.56	7.0	$\chi^2$	6
Q 1635+267	1.96	3.9	23.2	30	19.04	20.26	7.7	photo	7
SDSS J2336–0107	1.29	1.7	10.0	240	19.26	18.94	–	lens	8
Q 2345+007	2.16	7.1	42.4	480	18.68	20.45	0.3	$\chi^2$	9

NOTE. — The redshift of the binary quasar is  $z$ ,  $\Delta\theta$  is the angular separation,  $R$  is the proper transverse separation,  $|\Delta v|$  is the velocity difference between the two quasars in  $\text{km s}^{-1}$ ,  $i_1$  and  $i_2$  are extinction corrected  $i$ -band magnitudes of the brighter and fainter quasar respectively, and  $\chi^2$  is the value of our color similarity statistic, computed only for pairs with  $\Delta\theta > 3''$ . The last column labeled 'Sample' indicates which of our selection algorithms recovered the binary.

<sup>1</sup> (Pindor et al. 2005) SDSS binary quasar

<sup>2</sup> (Meylan & Djorgovski 1989) Q 1120+0195 is also named PHL 1222 and UM 144

<sup>3</sup> (Hagen et al. 1996). Spectra of both quasars are in the SDSS sample

<sup>4</sup> (Crampton et al. 1988) Both quasars are below the flux limit of the SDSS quasar survey.

<sup>5</sup> (Hewett et al. 1989)

<sup>6</sup> (Miller et al. 2004)

<sup>7</sup> (Sramek & Weedman 1978) This region of sky has been imaged by the SDSS but not yet spectroscopically observed. Both quasars are members of the faint photometric quasar sample

<sup>8</sup> (Gregg et al. 2002) SDSS binary quasar

<sup>9</sup> (Weedman et al. 1982)

optically unresolved in the SDSS imaging to avoid contamination from galaxies. Nearly all quasars at  $z > 0.70$  should be unresolved in the SDSS imaging, with the exception of very small separation pairs  $< 3''$ , however, these pair candidates are selected by our algorithm described in § 3.1.

We also used the criteria in eqn. (5) to search for pair candidates in the catalog of 273,287 faint photometric quasars. We restricted attention to members of the catalog only, and did not consider other nearby photometric objects. We will refer to binaries discovered in this catalog as our 'photometric sample'. The same criteria as in eqn (5) were used, but there were no lower or upper limits on redshift since spectroscopic redshifts are not available for this sample.

### 3.3. Overlap and Spectroscopic Selection

As mentioned previously, the SDSS contains a fair number of overlapping spectroscopic plates for which fiber collision does not limit the pair separation. Furthermore, quasar pairs can be found below the fiber collision limits by searching the SDSS+2QZ quasar catalog over regions where the survey areas overlap. Finally for separations  $\theta \geq 60''$ , larger than the SDSS fiber collision scale<sup>18</sup>, quasar pairs can be found in the entire SDSS area. We refer to pairs found in the spectroscopic catalog with  $\theta \leq 60''$  as our 'overlap' sample and we refer to those with  $\theta > 60''$  as our 'spectroscopic' sample. No color similarity criteria were applied to these objects, and the only magnitude or error limits are those imposed by the SDSS target selection (Richards et al. 2002a).

<sup>18</sup> Although the fiber collision limit is  $55''$ , for operational purposes we take it to be  $60''$  to give a small buffer from the actual limit where the fiber tiling may still be imperfect.

### 3.4. Previously Known Binaries

It is instructive to ask whether previously known binary quasars are selected by our selection techniques. In Table 1 we list the nine previously known binary quasars with  $0.7 \lesssim z \lesssim 3.0$  which are in the SDSS footprint, of which seven were recovered. The column labeled 'sample' indicates the sample for which each binary was selected as a candidate. Six of these binaries were listed in the compilation of binary quasars on the CASTLES<sup>19</sup> website. The others are SDSS J2336-0107 (Gregg et al. 2002) and SDSS J1120+6711 (Pindor et al. 2005), discovered recently in the SDSS search for gravitational lenses, and 2QZ J1435+0008, the  $33''$  pair of quasars discovered in the 2QZ by Miller et al. (2004).

Of the nine binaries listed in the table, all but Q 1343+2650, Q 1635+267, and 2QZ J1435+0008 had at least one member of the pair in the SDSS spectroscopic sample. Neither member of the pairs Q 1343+2650 and 2QZ 1435+0008 were targeted for spectroscopy because these quasars are below the flux limit of the SDSS quasar catalog ( $i < 19.1$  for quasars in this region of color space). The brighter member of Q 1635+267 is above the flux limit, but this area of sky has only been imaged and has yet to be spectroscopically observed. However, both members of this pair are members of the faint photometric catalog, and indeed, this pair was selected as a candidate by our photometric selection. Both members of the binary HS1216+5032 (Hagen et al. 1996) received SDSS fibers, so that this binary is a member of our overlap sample. The brighter of the two members of the famous double quasar Q 2345+0007 received an SDSS fiber, and this pair was selected as a pair candidate by our  $\chi^2$  algorithm. Of the two binaries which were not recovered,

<sup>19</sup> Available at <http://cfa-www.harvard.edu/castles>.



Q 1343+2650 was missed because it was below the SDSS flux limits and the quasar pair Q 1120+0195 (Meylan & Djorgovski 1989) was missed because its  $\chi^2 = 20.6$ , is just above the cutoff  $\chi^2 < 20$  of the ‘ $\chi^2$ ’ selection algorithm.

#### 4. SPECTROSCOPIC OBSERVATIONS

Candidates in our lens,  $\chi^2$ , and photometric samples require follow up spectroscopy to confirm the quasar pair hypothesis, which we describe in this section.

The SDSS images of the candidate quasar pairs and the spectrum of the quasar with an SDSS or 2QZ spectrum were visually inspected to reject bad imaging data and possible spectroscopic misidentifications. Color-color diagrams for each candidate were also visually inspected, and pairs for which the companion object overlaps the stellar locus (see e.g. Richards et al. 2001a) were given a lower priority.

The result of a successful follow up observation of a quasar pair candidate falls into one of four categories: (1) a quasar-quasar pair at the same redshift (2) a projected pair of quasars at different redshifts (3) a quasar-star pair (4) a star-star pair (for the photometric catalog). As an operational definition, we consider quasar pairs with velocity differences of  $|\Delta v| \leq 2000 \text{ km s}^{-1}$  to be at the same redshift, since this brackets the range of velocity differences caused by both peculiar velocities, which could be as large as  $\sim 500 \text{ km s}^{-1}$  if binary quasars reside in rich environments, and redshift uncertainties caused by blueshifted broad lines ( $\sim 1500 \text{ km s}^{-1}$ ) (Richards et al. 2002b).

Spectra of the vast majority of our quasar pair candidates were obtained with the Astrophysical Research Consortium (ARC) 3.5m telescope at the Apache Point Observatory (APO), during a number of nights between March 2003 and January 2005. In addition, two of the binary quasars in our sample were confirmed at other telescopes: SDSSJ1600+0000 was confirmed at the ESO 3.58m New Technology Telescope, and SDSSJ1028+3929 was discovered at the Hobby-Eberly Telescope. Higher signal to noise ratio spectra of five of the binary quasars in our sample were obtained at the 10m Keck I & Keck II telescopes.

For the ARC 3.5m observations, we used the Double Imaging Spectrograph (DIS), a double spectrograph with a transition wavelength of 5350 Å between the blue and red side. The observations were taken with low resolution gratings, with a dispersion of  $2.4 \text{ Å pixel}^{-1}$  in the blue side and  $2.3 \text{ Å pixel}^{-1}$  on the red side, and a resolution of roughly 2 pixels. A  $1.5''$  slit was used and we oriented the slit at the position angle between the two quasars so that both members of the pair could be observed simultaneously. The final spectrum covers the wavelength range of 3800 Å to 10,000 Å. The wavelength scale is calibrated with a polynomial fit to lines from an Ar-He-Ne lamp; the typical rms error of the fits is smaller than 0.5 Å. Observations of a variety of optical spectrophotometric standards (Oke & Gunn 1983) provided flux calibration; however, most of the candidates were not observed under photometric conditions, nor were they observed with the slit oriented at the parallactic angle. Exposure times ranged from 1200 seconds for candidates with  $i \sim 18$  to 2400 seconds for the faintest candidates,  $i \sim 20.8$ .

The binary quasar SDSSJ1600+0000 was discovered at the ESO New Technology Telescope 3.58m on UT 2001 April 18, using the red CCD of the ESO Multi-Mode Instrument (EMMI). The #13 grating ( $2.66 \text{ Å/pixel}$ ,  $R \simeq 600$  at 6000 Å) was used with an OG530 blue-blocking filter. Relative spectrophotometric calibration was obtained through observations of GD 108 (Oke 1990), but this calibration is uncertain blueward of 5350 Å and redward of 9300 Å.

The binary SDSSJ1028+3939 was identified from observations obtained using the Marcario Low Resolution Spectrograph (Hill et al. 1998) on the Hobby-Eberly Telescope (HET) on UT 2005 January 14. The HET observations were obtained with a  $300 \text{ line mm}^{-1}$  grating and GG385 blocking filter. Spectra of both components were obtained simultaneously using a  $1.5''$  slit. The spectra covered the range 4400-8000 Å at a resolution of 18 Å.

Higher signal to noise ratio spectra of both components of the quasar pairs SDSSJ0955+6045, SDSSJ1010+0416, and SDSSJ1719+2549 were obtained on UT 2003 February 5-6, using the Echelle Spectrograph and Imager (ESI; Epps & Miller 1998) on the Keck II telescope. The seeing was  $0''.6$ . The ESI has a dispersion of  $0.15 - 0.3 \text{ Å pixel}^{-1}$  over a wavelength range of 4000 – 10500 Å, and the  $1''$  slit used for these observations projects to 6.5 pixels. The 900s exposures were obtained with the slit aligned at the position angle of the components of the pair.

Spectra of both quasars in the pair SDSSJ0248+0009 were obtained on UT 1999 October 17 using the Low-Resolution Imaging Spectrograph Keck II telescope (LRIS; Oke et al. 1995), which was before LRIS was commissioned as a double spectrograph. The  $300 \text{ line mm}^{-1}$  grating blazed at 5000 Å was used, giving a spectral coverage of 5220 Å and a dispersion of  $2.55 \text{ Å pixel}^{-1}$ . The  $0''.7$  longslit was used and the seeing was  $0''.6$ . A single 900s exposure was obtained with the slit aligned at the position angle of the components of the pair.

We obtained spectra of both quasars in the pair SDSSJ0048-1051 on UT 2003 September 27 using the LRIS Double Spectrograph on the Keck I telescope. The D560 dichroic was used, which splits light between the blue arm and the red arm at 5600 Å. On the blue side, the  $600 \text{ line mm}^{-1}$  grism blazed at 4000 Å was used, giving a spectral coverage of 2590 Å and a dispersion of  $0.63 \text{ Å pixel}^{-1}$ . On the red side, the  $400 \text{ line mm}^{-1}$  grating was used blazed at 8500 Å, giving a spectral coverage of 3810 Å and a dispersion of  $1.86 \text{ Å pixel}^{-1}$ . The  $1''.0$  longslit was used and the seeing was  $0''.6$ . A single 900s exposure was obtained at an airmass of 1.2 with the slit aligned at the position angle of the components of the pair.

All the data were reduced using standard procedures in the IRAF<sup>20</sup> package, supplemented by IDL routines borrowed from the SDSS spectroscopic reduction software and adapted to the different instruments. Quasar redshifts were determined by cross correlating the quasar spectra with the first four eigenspectra of a principal component decomposition of the SDSS quasar sample (Schlegel et al. 2005).

<sup>20</sup> IRAF is distributed by the National Optical Astronomy Observatories, which are operated by the Association of Universities for Research in Astronomy, Inc., under cooperative agreement with the National Science Foundation.

In this section we present a sample of 218 new quasar pairs with transverse separations  $R_{\text{prop}} < 1 h^{-1}$  Mpc over the redshift range  $0.5 \leq z \leq 3.0$ . Of these, 65 have angular separations  $\theta \leq 60''$ , i.e. below the SDSS fiber collision scale. Our 26 new binaries with transverse proper separations  $R_{\text{prop}} < 50 h^{-1}$  kpc ( $\theta < 10''$ ) more than doubles the number of known binary quasars with separations this small. Table 2 lists relevant quantities for 33 binaries with  $3'' < \theta \leq 60''$  discovered from our  $\chi^2$  and photometric samples. The last column indicates which algorithm which was used to select the binary. The binaries with  $\theta \leq 3''$  discovered from our lens sample are shown in Table 3, and the overlap and spectroscopic binaries found by searching for pairs in the SDSS+2QZ quasar catalog are shown in Table 4. Table 5 gives a summary of the number of binary quasars selected by each algorithm described in § 3. For completeness, the Appendix includes tables of projected pairs of quasars at different redshifts, as well as projected quasar-star pairs.

The distribution of redshifts and proper transverse separations probed by these binary quasars is illustrated by the scatter plot in Figure 3. The (magenta) upside down triangle are members of the lens sample, the (green) squares are members of the photometric sample, and (red) triangle are in the  $\chi^2$  sample. The (blue) open circles are members of the overlap sample and smaller (blue) dots are pairs in the spectroscopic sample. The dashed curve shows the proper transverse distance corresponding to  $\theta = 3''$ , which divides the lens sample from the other samples, and the dotted line indicates the distance corresponding to  $\theta = 60''$ , above the fiber collision limit so that pairs can be found in the spectroscopic quasar catalog. It should be noted that the distribution of points in Figure 3 reflects some biases in our observational program. In particular, we tended to observe small separation pairs first, and we were much more likely to observe candidates with  $z > 2$ , because quasar pairs at these redshifts are of interest for studying the Ly $\alpha$  forest (Hennawi, et al. 2005).

We next discuss the possibility that some of the quasar pairs in this sample are strong gravitational lenses rather than binaries. After showing spectra of some of the more notable binaries, we define a sub-sample of binaries selected homogeneously which we will use in our analysis of small scale quasar clustering in § 6.

### 5.1. Contamination by Gravitational Lenses

It is possible that some of the quasar pairs with image splittings  $\lesssim 15''$  in our sample could be wide separation strong gravitational lenses rather than binary quasars. Indeed, the recently discovered quadruply imaged lensed quasar SDSSJ1004+4112 (Inada et al. 2003; Oguri et al. 2004) with a maximum image separation of  $14''.6$  was discovered as part of our follow up campaign to discover quasar pairs, as were two new gravitational lenses with separations  $\gtrsim 3''$  (Oguri et al. 2005). We thus review the set of objective criteria that must be satisfied for a quasar pair to be classified as a binary or lens (Kochanek, Falco, & Muñoz 1999; Mortlock, Webster, & Francis 1999) and briefly discuss why we have concluded that the binary hypothesis is correct for our pairs.

A quasar pair can be positively confirmed as a binary if

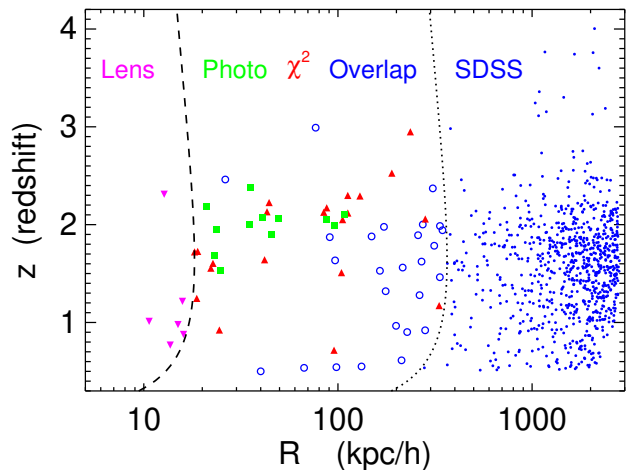


FIG. 3.— Range of redshifts and proper transverse separations probed by the binary quasars published in this work (see Tables 2, 3, 4, and 5). The blue circles are binary quasars identified in the SDSS spectroscopic sample. The region to the left of the dotted curve is excluded because of fiber collisions ( $\theta < 60''$ ), with the exception of the binaries discovered from overlapping plates, which are indicated by the larger open blue circles. The magenta circles are members of the lens sample, red circles are from the  $\chi^2$  sample, and green squares are binaries from the photometric sample. Because of the fiber collisions, the vast majority of small separation pairs  $R \lesssim 300 h^{-1}$  kpc were discovered from our follow-up observations. The dashed curve indicates the transverse separation corresponding to  $\theta = 3''$  below which binaries are found with our lens algorithm. Although we publish only pairs with separations  $R_{\text{prop}} < 1 h^{-1}$  Mpc in this work, Figure 3 shows all pairs in the SDSS+2QZ catalog out to  $3 h^{-1}$  Mpc for the sake of illustration.

the spectra of the images are vastly different (c.f. Gregg et al. 2002), if only one of the images is radio-loud (an  $O^2R$  pair, in the notation of Kochanek, Falco, & Muñoz 1999), or if the quasars' hosts are detected and they are not clearly lensed. The sufficient conditions for a pair to be identified as a lens are the presence of more than two images in a lensing configuration, the measurement of a time delay between images, the detection of a plausible deflector, or the detection of lensed host galaxy emission.

For the majority of pairs in our sample, the APO discovery spectra have too low a signal to noise ratio to make convincing arguments for or against the lensing hypothesis based on spectral dissimilarity. The exceptions are the five binaries for which we have high signal to noise ratio Keck spectra (three from ESI and two from LRIS). We comment on the spectral similarity of these binaries below.

Although the *absence* of a deflector in images of a quasar pair does not strictly speaking confirm the binary hypothesis, it certainly makes it more plausible. For small separation ( $\Delta\theta \lesssim 3''$ ) gravitational lenses, the lens galaxies are rarely detected in the relatively shallow SDSS imaging. However, for the wider separation lenses with  $\Delta\theta \gtrsim 3''$ , like SDSSJ1004+4112 ( $\Delta\theta_{\text{max}} = 14.62''$ ,  $z_{\text{lens}} = 0.68$ ) or Q 0957+561 ( $\Delta\theta = 6.2''$ ,  $z_{\text{lens}} = 0.36$ ; Walsh, Carswell, & Weymann 1979), where the lens is a bright galaxy in a cluster or group, the lens galaxies are detected in the SDSS imaging, though it is quite possible that fainter high redshift lens galaxies or clusters in

other wide separation lens systems would go undetected.

Using the University of Hawaii 2.2m telescope, we have taken deeper optical ( $i \lesssim 24$ ;  $z \lesssim 22$ ) or near infrared images ( $J \lesssim 22$ ;  $H \lesssim 22$ ) of all the binaries in our sample with separations  $\theta \leq 4''$  and of a subset of those with wider separations. None of the images showed lens galaxies in the foreground. For the wider  $\theta > 4''$  pairs, the lensing hypothesis would require a very bright massive galaxy in a group or cluster. In particular, because the typical redshift range of our binaries is  $z = 1.5 - 2$ , the most probable lens redshifts would be in the range  $z = 0.3 - 0.7$ , which would likely have been detected in the SDSS imaging. Furthermore, these wide separation multiply imaged quasars are extremely rare (Hennawi et al. 2005), thus we are confident that the pairs in our sample are all binaries.

### 5.2. Sample Spectra of Binaries

Keck ESI spectra of the three binaries SDSSJ0955+6045, SDSSJ1010+0416, and SDSSJ1719+2549 are shown in Figure 4. The signal to noise ratios of these spectra are high enough that we can make arguments against the lensing hypothesis based on spectral dissimilarity. In particular, for SDSSJ0955+6045 the narrow [OIII] emission lines are significantly stronger in one of the quasars than the other. In SDSSJ1010+0416, the CIII] emission lines have a velocity offset of  $\sim 2000 \text{ km s}^{-1}$ , although this offset is less apparent in MgII, which tends to be a better tracer of the systemic redshifts of quasars (Richards et al. 2002b). Finally, for SDSSJ1719+2549, the peak to continuum flux ratios of the MgII broad line differ by a factor of  $\sim 1.5$  between the two quasars.

Figure 5 shows Keck LRIS spectra of SDSSJ0048-1051 (moderate resolution) and SDSSJ0248+0009 (low resolution). For SDSSJ0048-1051 the profiles of all the emission lines differ significantly, especially MgII. For SDSSJ0248+0009, the peak to continuum flux ratios differ significantly for CIV, CIII], and MgII.

Figures 6 and 7 show SDSS and APO spectra of six other binaries in our sample.

### 5.3. Clustering Sub-sample

In this section, we define a statistical sub-sample of binary quasars which we will use to measure the quasar correlation function in §6. In §3, the various samples used to identify the binary quasars in Tables 2, 3, and 4 were described. These various selection algorithms selected quasar pairs over different angular scales, with different limiting magnitudes, and varying degrees of completeness. Here we combine these samples in a coherent way, which will allow us to quantify their selection function. We pay special attention to the completeness of each sample used and the parent sample of quasars searched to define each sample.

For the clustering analysis we restrict attention to quasars in the redshift range  $0.7 \leq z \leq 3.0$  with velocity differences  $|\Delta v| < 2000 \text{ km s}^{-1}$ . We use the lens,  $\chi^2$ , overlap, and spectroscopic samples. Our approach is to stitch the samples together as a function of angle. The photometric quasar pairs are not in the SDSS+2QZ catalog so the selection function and completeness of these binaries is more difficult to quantify.

All pairs with  $\theta \leq 3''$  come from the lens sample. The parent sample of quasars for this angular range is the 39,142 SDSS quasars to which we applied the lens algorithm. The completeness is the product of the *intrinsic* completeness of the lens algorithm (Pindor et al. 2003; Inada et al. 2003) and the fraction of candidates which have had spectroscopic confirmation thus far in the survey.

For pairs in the range  $3'' < \theta \leq 60''$  we use the  $\chi^2$  sample. Quasar pairs from the overlap sample which *also* meet the  $\chi^2$  selection criteria in eqn. (5) are included, and can be thought of as follow up observations which came for ‘free’ from the overlapping plates. Of the 21 binaries with  $0.7 \leq z \leq 3.0$  in the overlap sample, 8 satisfy  $\chi^2 < 20$  (see Table 4), and are included in the clustering sub-sample. The completeness of binary quasars in the range  $3'' < \theta \leq 60''$  is the product of completeness of the  $\chi^2$  selection,  $C(z|\chi^2 < 20)$ , and the fraction of candidates observed thus far. The parent sample around which we searched with the  $\chi^2$  algorithm is the combined SDSS+2QZ quasar sample of 59,608 quasars in the range  $0.7 \leq z \leq 3.0$ .

For separations  $\theta > 60''$ , we use pairs found in the SDSS spectroscopic catalog of 52,279 quasars. We restrict attention to the SDSS (rather than SDSS+2QZ), because the completeness for detecting quasar companions is very high if we restrict attention to companions above the SDSS flux limit for low redshift quasars. Vanden Berk et al. (2005) measured a completeness of  $\sim 95\%$  for quasars in the range  $0.3 < z < 3.0$  with  $i < 19.1$ . Thus we only include quasar pairs  $\theta > 60''$  in our clustering sample provided that *at least one* member of the pair is brighter than this flux limit.

Finally, any of the previously known binaries listed in Table 1 which satisfied any of the criteria for the clustering sub-sample are also included. Thus we include the binaries SDSS J1120+6711 and SDSS J2336-0107 as part of the lens sample, and LBQS 1429-0008, Q 2345+007, and 2QZ 1435+0008 are included as part of our  $\chi^2$  sample.

Of the 65 quasar pairs with angular separations  $\theta \leq 60''$  which we publish in this work, 35 are included in our clustering sub-sample along with five previously known binaries for a total of 40 sub-arcminute pairs. The distribution of redshifts and proper transverse separations of our clustering sample is illustrated by the scatter plot in Figure 8. The horizontal long-dashed lines indicate the redshift limits  $0.7 \leq z \leq 3.0$  of the sample, and the symbols and dotted and short dashed curves are the same as in Figure 3.

## 6. CLUSTERING ANALYSIS

A measurement of quasar clustering on the small scales probed by our binary sample  $10 h^{-1} \text{ kpc} \lesssim R_{\text{prop}} \lesssim 1 h^{-1} \text{ Mpc}$  is unprecedented. Our strategy has been to overcome the fiber collision limitation and high level of shot noise by following up close pairs of quasars to magnitudes  $i < 21$  fainter than the flux limit of the SDSS quasar survey.

As our pairs have a fainter flux limit than the underlying parent quasar catalog, and the mean density at this limit cannot be determined from the brighter sample, we cannot use the conventional technique of Monte Carlo integration of a random catalog to compute the corre-

TABLE 2  
 BINARY QUASARS WITH SEPARATIONS  $3'' < \Delta\theta < 60''$  DISCOVERED FROM FOLLOW-UP OBSERVATIONS

Name	RA (2000)	Dec (2000)	$u$	$g$	$r$	$i$	$z$	$\Delta\theta$	$z$	$\Delta v$	$R_{\text{prop}}$	$\chi^2$	Sample
SDSSJ0048-1051A	00:48:00.77	-10:51:48.6	20.99	20.52	20.18	19.94	19.91	3.6	1.56	< 200	22.1	5.8	$\chi^2$
APOJ0048-1051B	00:48:00.96	-10:51:46.2	20.39	20.04	19.70	19.30	19.28						
SDSSJ0054-0946A	00:54:08.47	-09:46:38.3	18.17	17.90	17.71	17.51	17.31	14.1	2.13	-1600	84.5	17.5	$\chi^2$
APOJ0054-0946B	00:54:08.04	-09:46:25.7	20.87	20.70	20.37	20.11	19.74						
SDSSJ0201+0032A	02:01:43.49	+00:32:22.7	19.99	19.39	19.47	19.41	19.19	19.0	2.30	-520	112.4	10.8	$\chi^2$
APOJ0201+0032B	02:01:42.25	+00:32:18.5	20.80	20.30	20.14	20.12	19.92						
SDSSJ0248+0009A	02:48:20.80	+00:09:56.7	19.44	19.24	19.23	18.98	19.00	6.9	1.64	< 200	41.9	8.8	$\chi^2$
APOJ0248+0009B	02:48:21.26	+00:09:57.3	20.77	20.71	20.74	20.57	20.39						
APOJ0332-0722A	03:32:38.38	-07:22:15.9	20.24	20.29	20.00	19.78	19.63	18.1	2.10	960	108.4	5.0	photo
APOJ0332-0722B	03:32:37.19	-07:22:19.6	20.63	20.57	20.22	19.96	19.70						
SDSSJ0846+2749A	08:46:31.77	+27:49:21.9	19.55	19.57	19.66	19.49	19.26	18.8	2.12	-490	112.4	14.3	$\chi^2$
APOJ0846+2749B	08:46:30.38	+27:49:18.1	19.82	19.88	19.82	19.71	19.55						
SDSSJ0939+5953A	09:39:48.78	+59:53:48.7	20.40	19.85	19.80	19.79	19.45	32.6	2.53	290	189.4	9.3	$\chi^2$
APOJ0939+5953B	09:39:46.56	+59:53:20.7	19.31	18.67	18.57	18.56	18.42						
SDSSJ0955+6045A	09:55:24.37	+60:45:51.0	20.84	20.37	20.29	20.25	20.34	18.6	0.72	460	95.5	10.8	$\chi^2$
APOJ0955+6045B	09:55:25.37	+60:45:33.8	20.68	20.65	20.62	20.72	20.30						
APOJ0959+5449A	09:59:07.46	+54:49:06.7	20.26	20.06	19.95	19.76	19.73	3.9	1.95	200	23.8	18.9	photo
APOJ0959+5449B	09:59:07.05	+54:49:08.4	20.48	20.61	20.43	20.28	19.82						
SDSSJ1010+0416A	10:10:04.98	+04:16:36.2	20.18	20.08	20.00	19.87	20.08	17.2	1.51	< 200	104.3	6.5	$\chi^2$
APOJ1010+0416B	10:10:04.37	+04:16:21.6	20.29	20.19	20.03	19.87	19.94						
SDSSJ1014+0920A	10:14:11.43	+09:20:47.7	19.95	19.14	19.12	18.92	18.73	22.0	2.29	< 200	129.8	11.7	$\chi^2$
APOJ1014+0921B	10:14:10.29	+09:21:01.7	20.81	20.27	20.25	20.13	19.79						
HETJ1028+3929A	10:28:43.67	+39:29:36.9	19.96	19.90	19.95	19.57	19.49	7.5	1.89	-1030	45.6	6.4	photo
HETJ1028+3929B	10:28:44.30	+39:29:34.8	20.92	20.81	20.91	20.60	20.66						
SDSSJ1034+0701A	10:34:51.47	+07:01:21.2	19.86	19.47	18.94	19.04	19.08	3.1	1.25	850	18.7	9.7	$\chi^2$
APOJ1034+0701B	10:34:51.38	+07:01:24.0	21.20	21.26	21.08	20.89	20.99						
2QZJ1056-0059A	10:56:44.89	-00:59:33.4	20.16	19.92	19.89	19.80	19.59	7.2	2.13	-350	43.1	6.7	$\chi^2$
APOJ1056-0059B	10:56:45.25	-00:59:38.1	20.76	20.78	20.59	20.58	20.33						
SDSSJ1123+0037A	11:23:10.96	+00:37:45.2	19.02	19.03	18.90	18.98	19.08	56.3	1.17	-330	332.1	6.0	$\chi^2$
APOJ1123+0037B	11:23:07.21	+00:37:45.7	20.26	20.29	20.10	20.12	20.22						
APOJ1225+5644A	12:25:45.73	+56:44:40.7	20.05	19.28	19.44	19.35	19.07	6.0	2.38	970	35.4	20.7	photo
APOJ1225+5644B	12:25:45.24	+56:44:45.1	21.08	20.52	20.50	20.35	19.80						
SDSSJ1254+6104A	12:54:21.98	+61:04:22.0	19.24	19.06	19.01	18.92	18.74	17.6	2.05	-1010	105.6	11.4	$\chi^2$
APOJ1254+6104B	12:54:20.52	+61:04:36.0	19.67	19.56	19.47	19.28	19.14						
APOJ1259+1241A	12:59:55.62	+12:41:53.8	20.33	19.99	19.93	19.74	19.53	3.6	2.19	-840	21.2	6.0	photo
APOJ1259+1241B	12:59:55.46	+12:41:51.0	20.22	19.90	19.87	19.79	19.56						
APOJ1303+5100A	13:03:26.17	+51:00:47.5	20.46	20.33	20.28	20.05	20.03	3.8	1.68	220	23.0	4.0	photo
APOJ1303+5100B	13:03:26.13	+51:00:51.3	20.87	20.60	20.66	20.38	20.59						
SDSSJ1310+6208A	13:10:37.89	+62:08:21.6	18.87	18.77	18.63	18.57	18.35	46.9	2.06	-1850	281.7	10.8	$\chi^2$
APOJ1310+6208B	13:10:31.96	+62:08:43.5	20.65	20.49	20.35	20.15	20.12						
SDSSJ1337+6012A	13:37:13.13	+60:12:06.7	18.68	18.57	18.56	18.34	18.42	3.1	1.73	-610	18.9	0.6	$\chi^2$
APOJ1337+6012B	13:37:13.08	+60:12:09.8	20.15	20.01	20.03	19.66	19.80						
SDSSJ1349+1227A	13:49:29.84	+12:27:07.0	17.92	17.76	17.71	17.46	17.45	3.0	1.72	< 200	18.3	12.9	$\chi^2$
APOJ1349+1227B	13:49:30.00	+12:27:08.8	19.50	19.26	19.10	18.74	18.60						
APOJ1400+1232A	14:00:52.07	+12:32:35.2	20.41	20.28	20.27	20.13	19.88	14.6	2.05	1470	87.7	0.6	photo
APOJ1400+1232B	14:00:52.56	+12:32:48.0	20.54	20.42	20.45	20.27	19.99						
SDSSJ1405+4447A	14:05:01.94	+44:47:59.9	18.68	18.14	17.93	17.86	17.66	7.4	2.23	1870	44.2	3.2	$\chi^2$
APOJ1405+4447B	14:05:02.41	+44:47:54.4	20.61	20.12	19.96	19.89	19.60						
APOJ1409+3919A	14:09:53.74	+39:19:60.0	20.31	20.24	20.14	20.06	19.78	6.8	2.08	480	40.7	3.9	photo
APOJ1409+3919B	14:09:53.88	+39:19:53.4	20.89	20.92	20.87	20.67	20.31						
APOJ1530+5304A	15:30:38.56	+53:04:04.2	20.86	20.54	20.42	20.13	20.06	4.1	1.53	230	25.0	8.8	photo
APOJ1530+5304B	15:30:38.82	+53:04:00.8	20.67	20.66	20.53	20.31	20.21						
SDSSJ1546+5134A	15:46:10.55	+51:34:29.5	22.34	20.57	20.31	20.20	20.29	42.2	2.95	-1450	236.0	12.4	$\chi^2$
APOJ1546+5134B	15:46:14.24	+51:34:05.0	20.64	19.43	19.10	18.91	18.88						
SDSSJ1629+3724A	16:29:02.59	+37:24:30.8	19.47	19.26	19.10	19.16	19.06	4.4	0.92	< 200	24.5	15.9	$\chi^2$
APOJ1629+3724B	16:29:02.63	+37:24:35.2	19.50	19.41	19.28	19.38	19.31						
SDSSJ1719+2549A	17:19:46.66	+25:49:41.2	20.17	19.93	19.90	19.85	19.61	14.7	2.17	-220	87.5	6.4	$\chi^2$
APOJ1719+2549B	17:19:45.87	+25:49:51.3	20.08	19.74	19.65	19.65	19.46						
SDSSJ1723+5904A	17:23:17.42	+59:04:46.8	19.40	19.04	18.95	18.69	18.76	3.7	1.60	-830	22.7	3.0	$\chi^2$
APOJ1723+5904B	17:23:17.30	+59:04:43.2	21.24	20.43	20.46	20.18	20.20						
APOJ2128-0617A	21:28:57.38	-06:17:50.9	19.84	19.66	19.87	19.80	19.68	8.3	2.07	-290	49.7	15.7	photo
APOJ2128-0617B	21:28:57.74	-06:17:57.2	20.03	19.74	20.12	19.92	19.63						
APOJ2214+1326A	22:14:27.03	+13:26:57.0	20.39	20.19	20.19	19.96	19.60	5.8	2.00	-690	35.2	19.4	photo
APOJ2214+1326B	22:14:26.79	+13:26:52.3	20.65	20.41	20.26	19.98	19.82						
APOJ2220+1247A	22:20:30.26	+12:47:33.5	20.11	20.03	20.00	19.88	19.78	15.9	1.99	1600	95.5	43.0	photo
APOJ2220+1247B	22:20:29.53	+12:47:45.1	20.92	20.85	20.72	20.34	20.21						

NOTE. — Quasars labeled SDSS or 2QZ are members of the SDSS or 2QZ spectroscopic quasar catalog and are designated as quasar ‘A’. Quasars discovered from follow up spectroscopy are labeled APO (or HET) and designated ‘B’. For pairs discovered from the photometric catalog, both quasars are labeled APO (or HET) and ‘A’ designates the brighter of the two quasars. Extinction corrected SDSS five band PSF photometry are given in the columns  $u$ ,  $g$ ,  $r$ ,  $i$ , and  $z$ . The redshift of quasar ‘A’ is indicated by column  $z$ ,  $\Delta\theta$  is the angular separation in arcseconds,  $\Delta v$  is the velocity of quasar B relative to quasar A in  $\text{km s}^{-1}$ ,  $R_{\text{prop}}$  is the transverse proper separation in  $h^{-1}$  kpc, and  $\chi^2$  is the value of our color similarity statistic. The last column labeled ‘Sample’ indicates the selection algorithm used to find the binary.

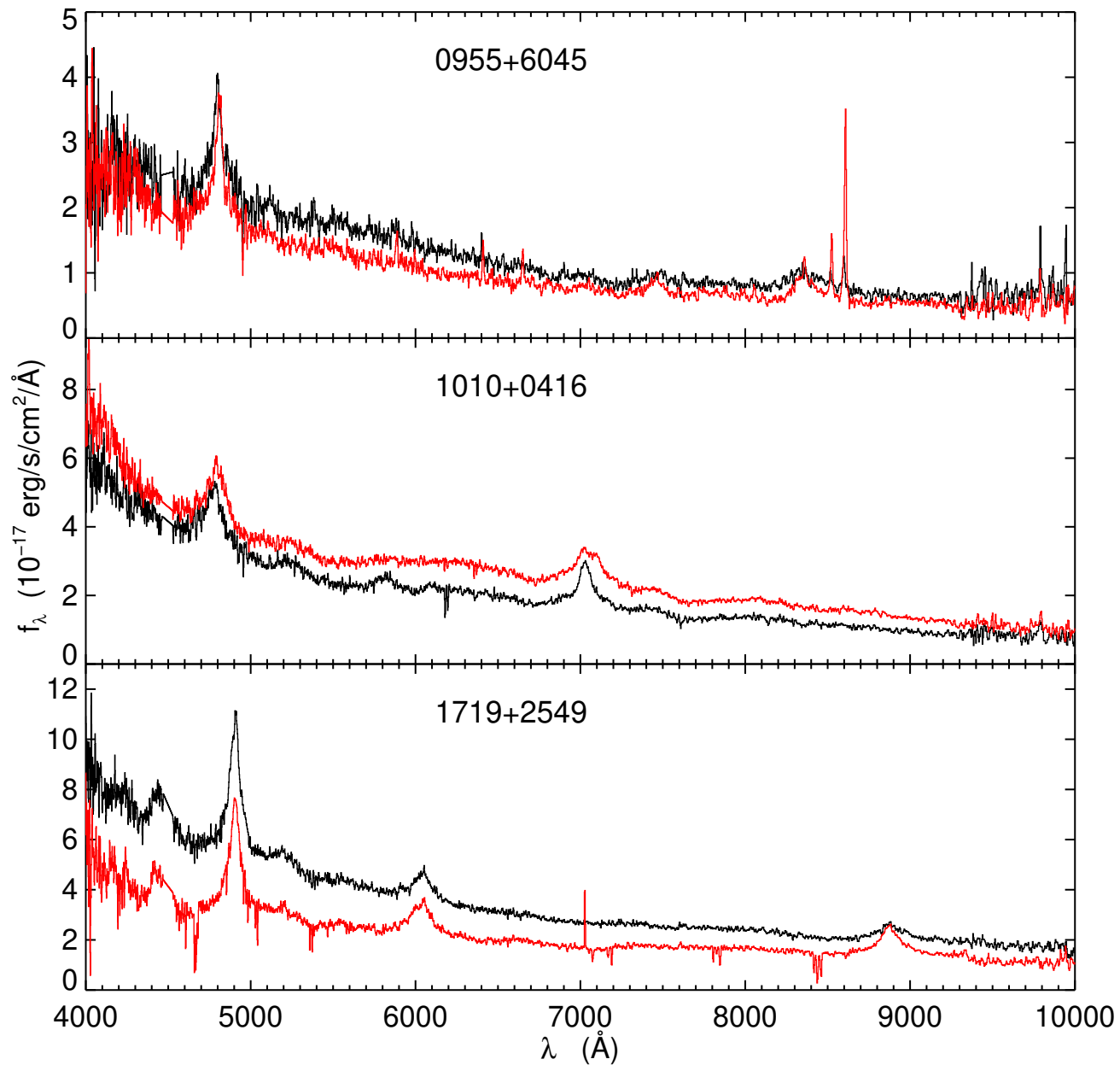


FIG. 4.— Keck ESI spectra of both members of three binary quasars. The top panel is the binary SDSSJ0955+6045 ( $z = 0.72$ ,  $\Delta\theta = 18''.6$ ,  $R_{\text{prop}} = 95.5 h^{-1} \text{ kpc}$ ), the middle panel is SDSSJ1010+0416 ( $z = 1.51$ ,  $\Delta\theta = 17''.2$ ,  $R_{\text{prop}} = 104.3 h^{-1} \text{ kpc}$ ), and the bottom panel is SDSSJ1719+2549 ( $z = 2.17$ ,  $\Delta\theta = 14''.7$ ,  $R_{\text{prop}} = 87.5 h^{-1} \text{ kpc}$ ). The discontinuity in the spectra at 4500 $\text{\AA}$  is an artifact of a gap in the Echelle orders.

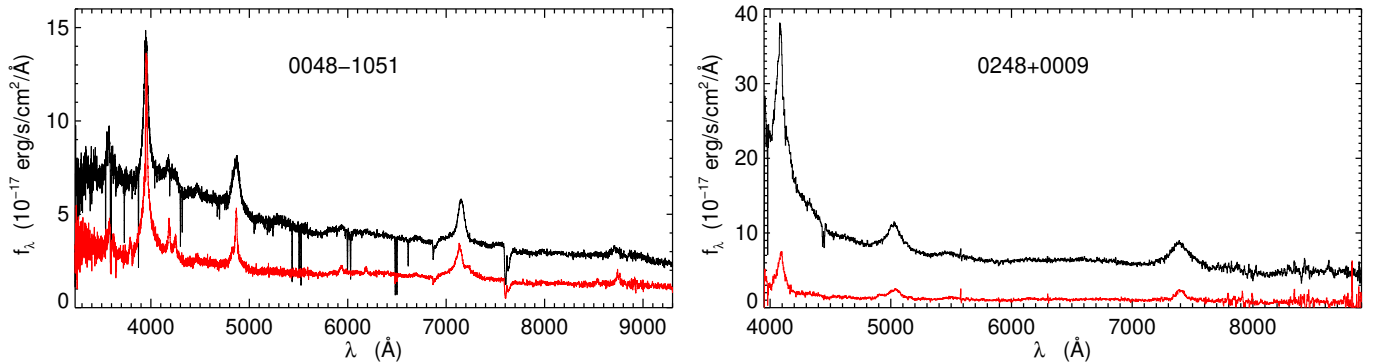


FIG. 5.— Keck spectra of two binary quasars. Spectral dissimilarity and the absence of a lensing galaxy in optical and near IR follow-up imaging provide strong evidence that these are both binary quasars rather than gravitational lenses. *Left*: Keck LRIS moderate resolution spectra of both members of the binary quasar SDSSJ0048-1051 ( $z = 1.56$ ,  $\Delta\theta = 3''.6$ ,  $R = 22.1 h^{-1}$  kpc). The absorption feature at  $7600\text{\AA}$  is telluric. *Right*: Keck LRIS low resolution spectra of both members of SDSSJ0248+0009 ( $z = 1.64$ ,  $\Delta\theta = 6''.8$ ,  $R = 41.9 h^{-1}$  kpc).

TABLE 3  
BINARY QUASARS WITH  $\Delta\theta < 3''$  DISCOVERED FROM LENS SELECTION

Name	RA (2000)	Dec (2000)	$u$	$g$	$r$	$i$	$z$	$\Delta\theta$	$z$	$\Delta v$	$R_{\text{prop}}$
SDSSJ0740+2926A	07:40:13.45	+29:26:48.4	18.61	18.46	18.30	18.42	18.48	2.6	0.98	230	15.0
APOJ0740+2926B	07:40:13.43	+29:26:45.7	19.98	19.67	19.50	19.68	20.03				
SDSSJ1035+0752A	10:35:19.37	+07:52:58.0	19.17	19.13	18.97	19.03	19.14	2.7	1.22	270	15.8
APOJ1035+0752B	10:35:19.23	+07:52:56.4	20.62	20.42	19.98	19.84	19.84				
SDSSJ1124+5710A	11:24:55.24	+57:10:57.0	19.34	18.66	18.83	18.65	18.44	2.2	2.31	-540	12.7
APOJ1124+5710B	11:24:55.44	+57:10:58.4	20.31	19.83	19.52	19.52	19.42				
SDSSJ1138+6807A	11:38:09.21	+68:07:38.8	18.28	17.98	17.87	17.89	17.78	2.6	0.77	840	13.7
APOJ1138+6807B	11:38:08.89	+68:07:36.9	20.31	19.74	19.76	19.72	19.58				
SDSSJ1508+3328A	15:08:42.21	+33:28:02.6	17.88	17.78	17.81	17.97	17.86	2.9	0.88	<200	16.0
APOJ1508+3328B	15:08:42.22	+33:28:05.5	20.56	20.36	20.15	20.56	19.71				
SDSSJ1600+0000A <sup>†</sup>	16:00:15.50	+00:00:45.5	19.23	19.11	18.84	18.95	19.08	1.9	1.01	-660	10.6
NTTJ1600+0000B <sup>†</sup>	16:00:15.59	+00:00:46.9	–	–	$\approx 21$	$\approx 21$	–				

NOTE. — Quasars labeled SDSS are the members of the SDSS spectroscopic quasar catalog and are designated as quasar ‘A’. Quasars discovered from follow up spectroscopy are labeled APO (or NTT) and designated ‘B’. Extinction corrected SDSS five band PSF photometry are given in the columns  $u$ ,  $g$ ,  $r$ ,  $i$ , and  $z$ . These magnitudes are estimated from the deblending algorithm of the main SDSS photometric pipeline (Stoughton et al. 2002) (except for 1600+0000 see below). The redshift of the SDSS quasar is given by  $z$ ,  $\Delta\theta$  is the angular separation in arcseconds,  $\Delta v$  is the the velocity of quasar B relative to quasar A in  $\text{km s}^{-1}$ , and  $R_{\text{prop}}$  is the transverse proper separation in  $h^{-1}$  kpc.

<sup>†</sup> The pair SDSSJ1600+0000A and NTTJ1600+0000B was not deblended by the photometric pipeline because the separation is too small. The magnitudes of SDSSJ1600+0000A have contributions from both members of the pair and the approximate  $r$  and  $i$  band magnitudes of NTTJ1600+0000B, were measured from follow up NTT imaging of this system.

lation function. However, the mean number density of quasars as a function of magnitude and redshift is well known (Croom et al. 2004a; Richards et al. 2005) and can be computed from the quasar luminosity function. Below, we explain how we model the quasar luminosity function. We then introduce an estimator for the quasar correlation function which takes the incompleteness of our pair survey into account. After determining the selection function of our clustering sub-sample, we compute its correlation function and compare it to previous clustering measurements extrapolated down to the scales  $R_{\text{prop}} \lesssim 1 h^{-1}$  Mpc probed by our binaries.

### 6.1. Modeling the Luminosity Function

At low redshift  $z < 2.3$ , the quasar luminosity function has been measured by several groups (Boyle et al. 2000; Croom et al. 2004b; Richards et al. 2005). We use the double power law B-band luminosity function (Boyle et

al. 2000)

$$\Phi(M_B, z) = \frac{\Phi_*$$

where  $\beta_l = -1.64$ ,  $\beta_h = -3.43$ , and  $\Phi_* = 360(h/0.50)^3 \text{Gpc}^{-3} \text{mag}^{-1}$ . The evolution of the break luminosity  $M_B^*(z)$  follows

$$M_B^* = M_B^*(0) - 2.5(k_1 z + k_2 z^2), \quad (6)$$

with  $k_1 = 1.36$ ,  $k_2 = -0.27$ , and  $M_B^*(0) = -21.15 + 5 \log h$ .

The quasar luminosity function is poorly constrained between redshifts  $2.6 \leq z \leq 2.9$ , because quasar colors cross the stellar locus (see e.g. Richards et al. 2001a), in this range and color selected samples suffer high incompleteness. As we desire to predict the number density of quasars in the redshift range  $0.7 < z < 3.0$  probed by our clustering sub-sample, we devise a simple interpolation scheme to cover the range  $2.3 < z < 3.0$ : Wyithe & Loeb (2002a) used a simple analytical model to fit

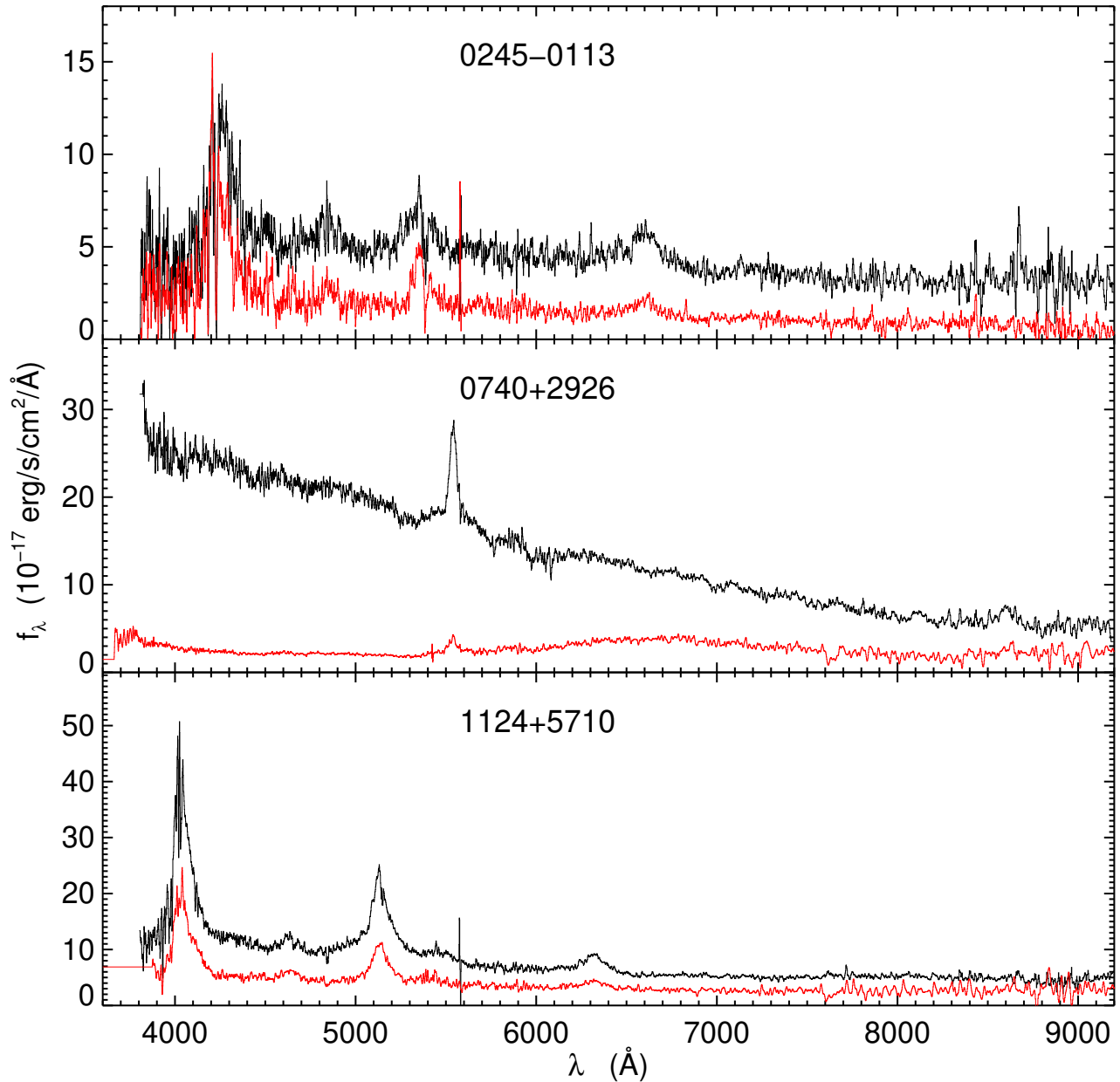


FIG. 6.— SDSS and APO spectra of both members of three binary quasars. The top panel is the binary SDSSJ0245-0113 ( $z = 2.46$ ,  $\Delta\theta = 4''.5$ ,  $R_{\text{prop}} = 26.3 h^{-1}$  kpc), the middle panel is SDSSJ0740+2926 ( $z = 0.98$ ,  $\Delta\theta = 2''.6$ ,  $R_{\text{prop}} = 15.0 h^{-1}$  kpc), and the bottom panel is SDSSJ1124+5710 ( $z = 2.31$ ,  $\Delta\theta = 2''.2$ ,  $R_{\text{prop}} = 12.7 h^{-1}$  kpc). The binary in the top panel was a member of our overlap sample, hence both quasars have SDSS spectra. For both the middle and bottom panels, the black curves are SDSS spectra of the brighter quasar in the pair and the red curves are the APO spectra of the fainter companions. The absorption feature at  $7600\text{\AA}$  in the lower two spectra is telluric. Although all three of these binaries have separations  $\Delta\theta \lesssim 5''$  characteristic of gravitational lenses, deep optical and near IR imaging show no lenses in the foreground.

the double power law luminosity function in eqn. (5) to both the Fan et al. (2001) high redshift ( $z > 3.6$ ) luminosity function and the Boyle et al. (2000) low redshift ( $z < 2.3$ ) luminosity function. For redshifts  $z < 2.3$  we use the Boyle et al. (2000) expression in eqn. (5). In the range  $2.3 < z < 3.0$  we simply linearly interpolate between eqn. 5 and the Wyithe & Loeb (2002a) fit. Since

the number of binary quasars in our clustering sample in this redshift range is relatively small, our conclusions will be insensitive to any uncertainties in this procedure.

Although the luminosity functions we are considering are expressed in terms of  $M_B$ , both the SDSS spectroscopic survey and our binary quasar survey have flux limits in the  $i$ -band. Thus in order to compute the num-

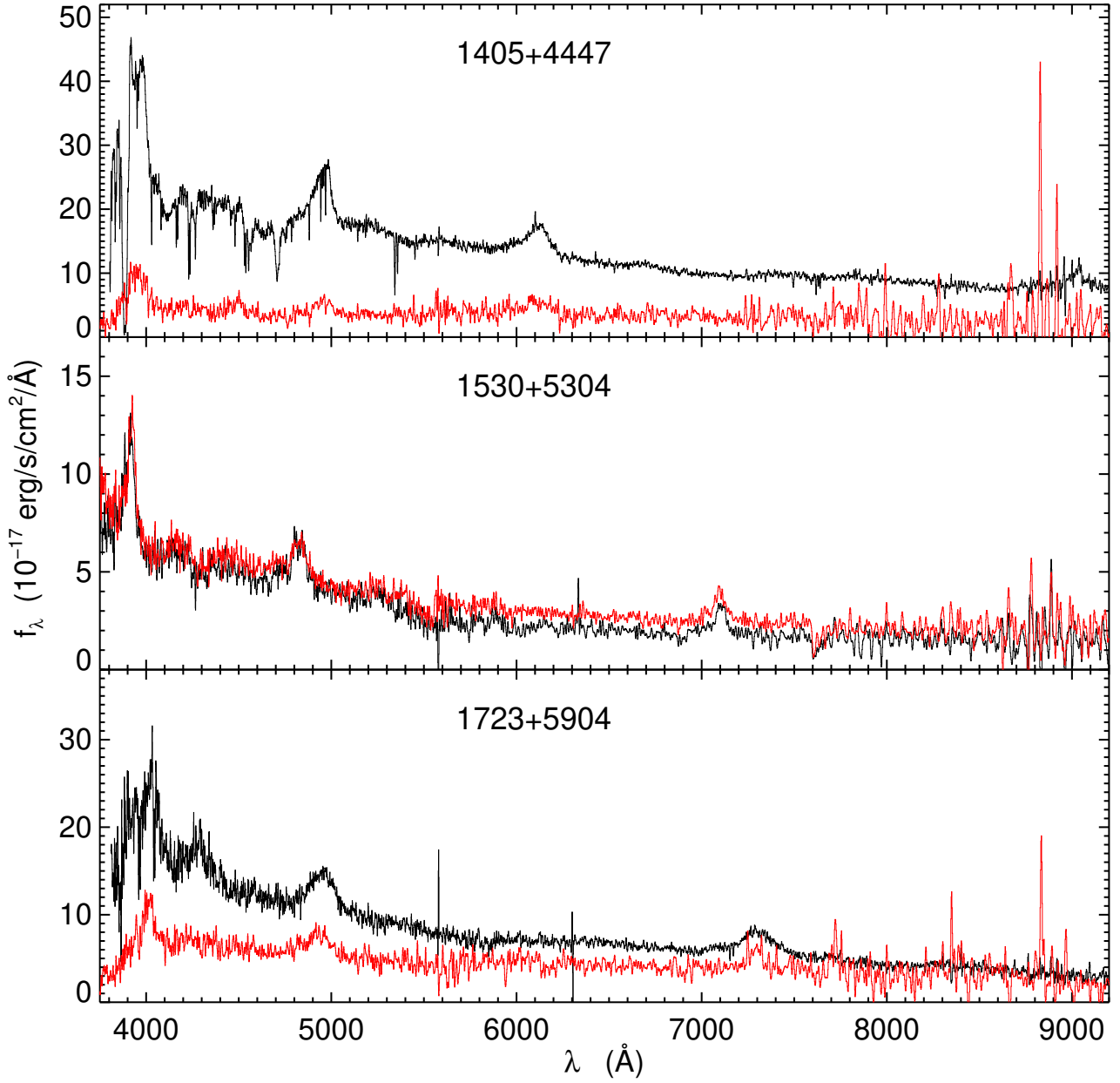


FIG. 7.— SDSS and APO spectra of both members of three binary quasars. The top panel is the binary SDSSJ1405+44447 ( $z = 2.23$ ,  $\Delta\theta = 7''.4$ ,  $R = 142.8 h^{-1}$  kpc), the middle panel is SDSSJ1530+5304 ( $z = 1.53$ ,  $\Delta\theta = 4''.1$ ,  $R = 63.3 h^{-1}$  kpc), and the bottom panel is SDSSJ1723+5904 ( $z = 1.60$ ,  $\Delta\theta = 3''.7$ ,  $R = 59.0 h^{-1}$  kpc). The binary in the middle panel is a member of the photometric sample, and both spectra were taken at APO. In the other two panels, the black curves are SDSS spectra of the brighter quasar in the pair and the red curves are the APO spectra of the fainter companion. Deep imaging of SDSSJ1405+44447 and SDSSJ1723+5904 shows no lens in the foreground. The absorption features at  $7600\text{\AA}$  are telluric.

ber of quasars above our flux limit, we need to know the cross filter K-correction  $K_{Bi}(z)$ , between apparent magnitude  $i$  and absolute magnitude  $B$  (see e.g. Hogg, Baldrý, Blanton, & Eisenstein 2002)

$$M_B^i = i - DM(z) - K_{Bi}(z) \quad (7)$$

where  $DM(z)$  is the distance modulus. We compute  $K_{Bi}(z)$  from the SDSS composite quasar spectrum of

Vanden Berk et al. (2001) and the Johnson-B and SDSS  $i$  filter curves.

The number density of quasars brighter than the flux limit  $i'$  is an integral over the luminosity function

$$n(z, i < i') = \int_{M_B^{\text{bright}}}^{M_B^{i'}} dM_B \Phi(M_B, z), \quad (8)$$

where  $M_B^{\text{bright}}(z)$  and  $M_B^{i'}(z)$  are the absolute magni-



TABLE 4  
 BINARY QUASARS DISCOVERED IN OVERLAPPING PLATES AND THE SDSS+2QZ CATALOG<sup>†</sup>

Name	RA (2000)	Dec (2000)	<i>u</i>	<i>g</i>	<i>r</i>	<i>i</i>	<i>z</i>	$\Delta\theta$	<i>z</i>	$\Delta v$	$R_{\text{prop}}$	$\chi^2$
SDSSJ0012+0052A	00:12:01.88	+00:52:59.7	21.53	20.82	20.33	19.83	19.63	16.0	1.63	1590	97.3	59.8
SDSSJ0012+0053B	00:12:02.35	+00:53:14.1	21.03	20.82	20.51	20.22	20.10					
SDSSJ0117+0020A	01:17:58.84	+00:20:21.5	17.96	17.67	17.82	17.79	17.99	44.5	0.61	-260	212.9	34.1
SDSSJ0117+0021B	01:17:58.00	+00:21:04.1	20.26	20.01	20.13	19.86	19.89					
SDSSJ0141+0031A	01:41:11.63	+00:31:45.9	20.23	20.19	20.11	19.87	19.96	42.9	1.89	1140	259.2	2.9
SDSSJ0141+0031B	01:41:10.41	+00:31:07.1	20.76	20.59	20.50	20.29	20.20					
SDSSJ0245-0113A	02:45:12.08	-01:13:14.0	20.56	19.85	19.56	19.47	19.33	4.5	2.46	-190	26.3	17.0
SDSSJ0245-0113B	02:45:11.90	-01:13:17.6	21.14	20.57	20.45	20.38	20.11					
SDSSJ0258-0003A	02:58:15.55	-00:03:34.2	18.93	18.93	18.66	18.66	18.74	29.4	1.32	240	176.6	32.9
SDSSJ0258-0003B	02:58:13.66	-00:03:26.5	19.67	19.89	19.66	19.75	19.71					
SDSSJ0259+0048A*	02:59:59.69	+00:48:13.7	19.63	19.26	19.22	19.33	19.10	19.6	0.89	830	108.1	1914.2
SDSSJ0300+0048B	03:00:00.57	+00:48:28.0	19.47	19.01	16.51	16.37	16.05					
SDSSJ0350-0031A	03:50:53.29	-00:31:14.7	20.35	20.17	19.45	18.99	18.62	45.5	2.00	-920	273.8	492.9
SDSSJ0350-0032B	03:50:53.05	-00:32:00.1	19.66	19.40	19.32	19.29	19.16					
SDSSJ0743+2054A	07:43:37.29	+20:54:37.1	20.06	19.86	19.77	19.51	19.43	35.5	1.56	640	215.5	15.9
SDSSJ0743+2055B	07:43:36.85	+20:55:12.1	20.36	20.08	20.04	19.90	19.94					
SDSSJ0747+4318A	07:47:59.02	+43:18:05.4	19.52	19.24	19.21	18.89	18.75	9.2	0.50	150	39.9	6.3
SDSSJ0747+4318B	07:47:59.66	+43:18:11.5	19.79	19.45	19.36	19.11	18.99					
SDSSJ0824+2357A	08:24:40.61	+23:57:09.9	18.72	18.51	18.69	18.58	18.59	14.9	0.54	-170	67.0	13.2
SDSSJ0824+2357B	08:24:39.83	+23:57:20.3	19.00	18.67	18.88	18.70	18.72					
SDSSJ0856+5111A	08:56:25.63	+51:11:37.4	18.90	18.52	18.64	18.45	18.51	21.8	0.54	60	98.2	138.9
SDSSJ0856+5111B	08:56:26.71	+51:11:18.2	20.03	19.55	19.42	19.17	19.19					
SDSSJ0909+0002A	09:09:24.01	+00:02:11.0	16.65	16.68	16.61	16.39	16.34	15.0	1.87	1700	90.6	28.0
SDSSJ0909+0002B	09:09:23.13	+00:02:04.0	20.08	20.06	20.11	19.97	19.82					
SDSSJ0955+0616A	09:55:56.38	+06:16:42.5	17.79	18.07	17.84	17.81	17.86	44.0	1.28	-1040	263.3	38.6
SDSSJ0955+0617B	09:55:59.03	+06:17:01.9	20.35	20.29	20.11	20.21	20.29					
SDSSJ1032+0140A	10:32:44.65	+01:40:20.5	18.93	18.86	18.84	18.76	18.86	55.1	1.46	-1580	333.5	16.0
2QZJ1032+0139B	10:32:43.17	+01:39:30.0	20.50	20.46	20.27	20.15	20.21					
SDSSJ1103+0318A	11:03:57.72	+03:18:08.3	18.35	18.36	18.30	18.10	17.96	57.3	1.94	-1730	345.7	41.5
SDSSJ1104+0318B	11:04:01.49	+03:18:17.5	19.08	19.04	19.12	19.02	18.97					
SDSSJ1107+0033A	11:07:25.70	+00:33:53.9	18.98	18.94	18.84	18.51	18.42	24.8	1.88	280	150.1	22.9
2QZJ1107+0034B	11:07:27.08	+00:34:07.6	20.01	20.04	20.05	19.84	19.80					
SDSSJ1116+4118A	11:16:11.74	+41:18:21.5	20.35	18.53	18.16	17.94	17.96	13.8	2.99	890	76.8	28.4
SDSSJ1116+4118B	11:16:10.69	+41:18:14.4	21.33	19.44	19.17	19.03	19.03					
SDSSJ1134+0849A	11:34:57.74	+08:49:35.3	19.30	19.10	19.01	18.83	18.85	27.1	1.53	-390	164.4	6.4
SDSSJ1134+0849B	11:34:59.38	+08:49:23.3	19.65	19.50	19.34	19.11	19.13					
2QZJ1146-0124A	11:46:52.97	-01:24:46.4	20.54	20.23	20.17	19.93	19.65	28.5	1.98	-490	172.0	26.0
2QZJ1146-0124B	11:46:51.19	-01:24:56.3	20.53	20.46	20.52	20.35	20.24					
SDSSJ1152-0030A	11:52:40.53	-00:30:04.3	18.95	18.80	18.93	18.86	18.80	29.3	0.55	740	132.8	23.1
2QZJ1152-0030B	11:52:40.10	-00:30:32.9	20.32	20.12	20.16	19.99	20.16					
SDSSJ1207+0115A	12:07:00.97	+01:15:39.4	19.03	18.94	18.84	18.87	18.85	35.4	0.97	-260	200.1	3.5
2QZJ1207+0115B	12:07:01.40	+01:15:04.7	20.62	20.40	20.30	20.37	20.36					
2QZJ1217+0006A	12:17:36.18	+00:06:57.4	19.96	19.93	20.06	19.76	19.62	51.8	1.78	-200	314.0	13.5
2QZJ1217+0006B	12:17:35.03	+00:06:08.6	19.17	19.30	19.32	19.05	19.17					
2QZJ1217+0055A	12:17:36.95	+00:55:22.7	20.33	20.24	20.12	20.23	19.84	40.5	0.90	-60	224.7	18.3
2QZJ1217+0055B	12:17:34.25	+00:55:22.2	20.25	19.92	19.78	19.82	19.98					
SDSSJ1226-0112A	12:26:24.09	-01:12:34.5	17.47	17.39	17.23	17.27	17.28	50.6	0.92	100	282.4	22.8
2QZJ1226-0113B	12:26:25.58	-01:13:19.9	19.74	19.82	19.75	19.79	19.53					
SDSSJ1300-0156A	13:00:45.56	-01:56:31.8	18.26	18.26	18.14	17.88	17.90	44.5	1.62	480	270.7	37.6
2QZJ1300-0157B	13:00:44.52	-01:57:13.5	19.81	19.72	19.73	19.59	19.70					
2QZJ1328-0157A	13:28:30.14	-01:57:32.8	19.86	19.49	19.52	19.55	19.42	52.6	2.37	-890	309.2	26.8
2QZJ1328-0157B	13:28:33.64	-01:57:27.9	20.46	19.92	19.78	19.77	19.75					
2QZJ1354-0108A	13:54:40.40	-01:08:45.4	19.48	19.54	19.46	19.29	19.21	55.5	1.99	740	334.2	37.1
2QZJ1354-0107B	13:54:39.97	-01:07:50.3	20.40	20.13	19.99	19.85	19.64					

NOTE. — Quasars labeled SDSS or 2QZ are members of the SDSS or 2QZ spectroscopic quasar catalog. The brighter of the two quasars is designated ‘A’, except for SDSS-2QZ pairs for which the SDSS quasar is designated ‘A’. Extinction corrected SDSS five band PSF photometry are given in the columns *u*, *g*, *r*, *i*, and *z*. The redshift of quasar ‘A’ is indicated by column *z*,  $\Delta\theta$  is the angular separation in arcseconds,  $\Delta v$  is the velocity of quasar B relative to quasar A in  $\text{km s}^{-1}$ ,  $R_{\text{prop}}$  is the transverse proper separation in  $h^{-1}$  kpc, and  $\chi^2$  is the value of our color similarity statistic.

<sup>†</sup> We publish all quasars with proper transverse separations  $R_{\text{prop}} < 1 h^{-1}$  Mpc, however only those with  $\theta < 60''$  are listed in this table. The entire sample of pairs is published in the electronic version of this article.

\* The quasar SDSSJ0300+0048B has a large BAL trough which explains the very large  $\chi^2 = 1914.2$  for this pair.

tudes corresponding to the bright and faint end apparent magnitude limits as per eqn. (7).

To check our model, we compute the cumulative number magnitude counts  $n(< i)$  for the redshift range  $0.3 < z < 3.0$  and compare to the measurement over

the same redshift interval by Vanden Berk et al. (2005). We find that our model slightly overestimates the number counts of quasars. Specifically, Vanden Berk et al. (2005) measured  $n(< 18.5) = 3.74 \text{ deg}^{-2}$  whereas our model predicts  $n(< 18.5) = 4.63 \text{ deg}^{-2}$ . We thus scale

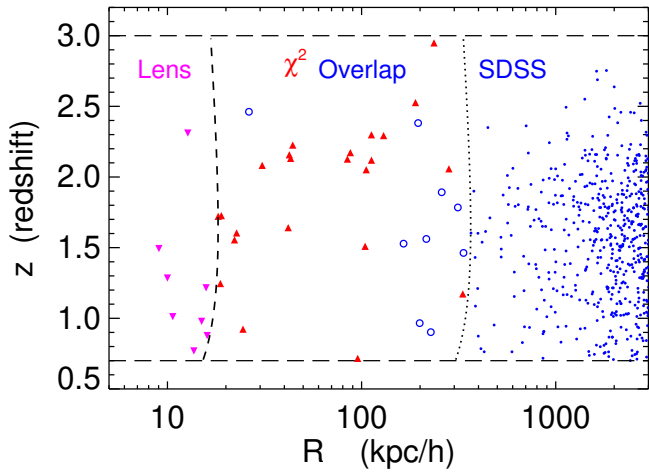


FIG. 8.— Range of redshifts and proper transverse separations probed by the binary quasars in our clustering sub-sample. The blue circles are binary quasars identified in the SDSS spectroscopic sample ( $\theta > 60''$ ). The short dashed line indicates the transverse separation corresponding to  $\theta = 60''$ . The open blue circles indicate pairs from the overlapping plates. These pairs are required to also meet the  $\chi^2$  selection criteria (eqn. 5). The magenta circles are members of the lens sample and red circles are from  $\chi^2$  sample. The dashed curve indicates the transverse separation corresponding to  $\theta = 3''$  below which binaries are found with our lens algorithm. The horizontal long dashed curves at  $z = 0.7$  and  $z = 3.0$  indicate the redshift limits of the clustering sub-sample.

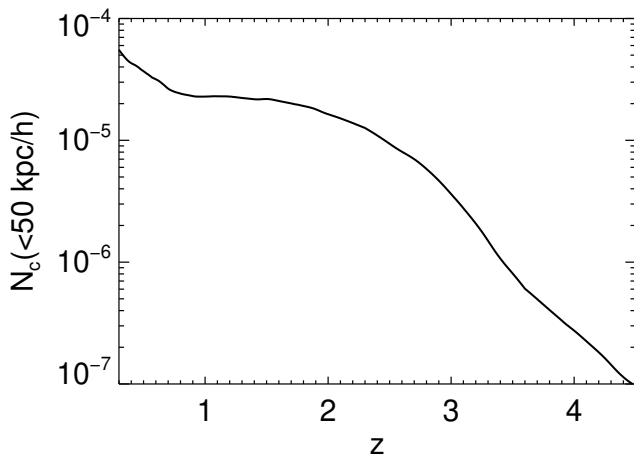


FIG. 9.— Expected mean number of companions per quasar with proper transverse separation  $R_{\text{prop}} < 50 h^{-1}$  kpc and velocity difference  $|\Delta v| < 2000 \text{ km s}^{-1}$ , as a function of redshift calculated from eqn. 16, which assumes the large scale quasar correlation function can be extrapolated as a power law to small scales. We used the correlation function parameters,  $\gamma = 1.53$  and  $r_0 = 4.8 h^{-1}$  Mpc, measured by PMN from the 2dF quasar survey. A perfect survey, with no sources of incompleteness, is assumed. In a sample of  $\sim 50,000$  quasars, the predicted number of binaries with  $R < 50 h^{-1}$  kpc is  $\sim 1$ . However, our clustering sample already contains 20 quasars with transverse separations this small, which is compelling evidence for excess clustering over what is expected from extrapolating the correlation function.

TABLE 5  
SUMMARY OF BINARY QUASAR SAMPLE

Algorithm	Number of Binaries
Lens	6
$\chi^2$	21
Photometric	12
Overlap	26
Spectroscopic	153

NOTE. — Number of binary quasars with  $R_{\text{prop}} < 1 h^{-1}$  Mpc, selected by the various algorithms discussed in § 3 and plotted in Figure 3.

our model luminosity function down by this ratio so as to give the correct number counts for  $i < 18.5$ .

### 6.2. Estimating the Correlation Function

If it is true that quasars depart from the gravitational clustering hierarchy because of dissipative encounters, this would be expected to occur for separations smaller than some length scale characteristic of tidal effects or mergers. Proper rather than comoving coordinates are appropriate for such an investigation. However, clustering measurements are typically carried out in comoving coordinates, as these are most intuitive in the linear regime where objects are still moving with the Hubble flow. We will compute the correlation function in both proper and comoving units, but for definiteness we use comoving units in the equations which follow.

We consider quasars with a maximum velocity difference of  $|\Delta v| < 2000 \text{ km s}^{-1}$ , thus we will measure the redshift space correlation function projected over this velocity interval

$$w_p(R, z) = \int_{-\frac{v_{\text{max}}}{aH(z)}}^{\frac{v_{\text{max}}}{aH(z)}} \xi_s(R, s, z) ds \quad (9)$$

where  $\xi_s$  is the quasar correlation function in redshift space,  $v_{\text{max}} = 2000 \text{ km s}^{-1}$ ,  $H(z)$  is the expansion rate at redshift  $z$ , and the factor of  $a = 1/(1+z)$  converts the redshift distance to comoving units.

The redshift space correlation function,  $\xi_s(R, s, z)$  is the convolution of the velocity distribution in the redshift direction,  $F_v(v_z)$ , with the real space correlation function  $\xi(r, z)$ ,

$$\xi_s(R, s, z) = \int_{-\infty}^{\infty} \xi(\sqrt{R^2 + x^2}, z) F_v(H(z)[x - s]) dx. \quad (10)$$

The radial velocity distribution  $F_v(v_z)$  has contributions from both peculiar velocities and uncertainties in the systemic redshifts of the quasars. Provided that the distance in redshift space over which we project contains most of the area under  $F_v$ , it is a good approximation to replace the redshift space correlation function,  $\xi_s$ , under the integral in eqn. (9) with the real space correlation function,  $\xi$ , since radial velocities will simply move pairs of points within the volume.

The small number of close pairs will limit the number of bins in  $R$  for which we can measure the correlation function. Since  $w_p$  may change significantly over these large bins, we choose to measure the volume averaged

projected correlation function integrated over each radial bin. We denote this dimensionless quantity by  $\bar{W}_p$ . Within a comoving bin  $[R_{\min}, R_{\max}]$  it can be written as:

$$\bar{W}_p(R_{\min}, R_{\max}, z) = \frac{\int_{-\frac{v_{\max}}{aH(z)}}^{\frac{v_{\max}}{aH(z)}} \int_{R_{\min}}^{R_{\max}} \xi(R, s, z) 2\pi R dR ds}{V_{\text{shell}}} \quad (11)$$

where  $V_{\text{shell}}$  is the volume of the cylindrical shell in redshift space

$$V_{\text{shell}} = \pi(R_{\max}^2 - R_{\min}^2) \left( \frac{2v_{\max}}{aH(z)} \right). \quad (12)$$

The correlation function of a point process is computed by comparing the number of pairs detected to the number expected in the absence of clustering, taking into account the sample limits. We choose the estimator

$$1 + \bar{W}_p(R_{\min}, R_{\max}) = \frac{\langle \text{QQ} \rangle}{\langle \text{QR} \rangle}. \quad (13)$$

Usually, random catalogs are constructed to determine the average number of data-random pairs  $\langle \text{QR} \rangle$ . However a subtlety arises in the current context because for  $\Delta\theta < 60''$ , we have targeted the companion quasars (i.e the quasar discovered from follow-up observations) to fainter magnitudes than the quasars from the parent spectroscopic sample. Rather than estimate the correlation function from the number of pairs, we use the number of *companions*. Specifically,  $\langle \text{QQ} \rangle$  is defined to be the number of companions about quasars in the parent sample in a given comoving transverse radial bin  $[R_{\min}, R_{\max}]$ , and  $\langle \text{QR} \rangle$  is the average number of random companions in this radial bin in the absence of clustering. In the case where the parent and companion samples are distinct (as is the case for the lens and  $\chi^2$  samples) then  $\langle \text{QQ} \rangle$  is just the number of binaries in the bin in question. However, if the parent and companion samples are identical (as is the case for the overlap and spectroscopic samples), then  $\langle \text{QQ} \rangle$  is *twice* the number of pairs, since each of the two quasars in the parent sample have a companion.

Our model of the luminosity function in the previous section is used to compute the average number of random companions R about the quasars Q in each parent quasar sample, taking into account the flux limits and various sources of incompleteness. We separately compute quasar-random contribution for each selection algorithm used to define our clustering sample and we then add the results. Specifically, for a comoving transverse radial bin  $[R_{\min}, R_{\max}]$ , centered on  $R$ , we can write

$$\langle \text{QR} \rangle = \sum_j^{N_{\text{qso}}} n(z_j, i < i') V_{\text{shell}} S(z_j, \theta_j), \quad (14)$$

where  $n(z, i < i')$  is the number density of quasars above the flux limit  $i'$ ,  $V_{\text{shell}}$  is the volume of each bin in eqn. (12), and the sum is over all quasars in the parent sample. The quantity  $S(z_j, \theta_j)$  is the selection probability of detecting a companion about the  $j$ th quasar. It is a function of angle and redshift since these quantities parameterize our various selection algorithms, as discussed in § 3. Here  $\theta_j = R/D(z)$  is the angle onto which the (logarithmic) center of the bin projects for a quasar at redshift  $z$ , and  $D(z)$  is the comoving distance.

In what follows we will compare our measured correlation function to previous larger scale ( $1 h^{-1}$  Mpc –  $30 h^{-1}$  Mpc) clustering measurements extrapolated as a power law down to the scales probed by our binaries. Since  $\bar{W}_p$  in eqn. (11) is a function of redshift, we must average it over the redshift distribution of our quasar sample before a comparison can be made to the measurement from eqn. (13),

$$\bar{W}_p(R_{\min}, R_{\max}) = \frac{1}{N_{\text{qso}}} \sum_j^{N_{\text{qso}}} \bar{W}_p(R_{\min}, R_{\max}, z_j) \quad (15)$$

PMN found that  $\xi(r)$  is well fit by a power law, with  $\gamma = 1.53$  and  $r_0 = 4.8 h^{-1}$  Mpc, for the 2dF sample taken as a whole. They also found  $r_0$  increases with redshift, from  $r_0 = 3.4 - 5.9 h^{-1}$  Mpc, which we take into account in eqn. (15).

In Figure 9 we show the prediction for the number of companions in the bin  $0 < R_{\text{prop}} < 50 h^{-1}$  kpc with  $|\Delta v| < 2000 \text{ km s}^{-1}$  as a function of redshift

$$N_c = n(z, i < 21) V_{\text{shell}} [1 + \bar{W}_p(0, 50 h^{-1} \text{ kpc}, z)]. \quad (16)$$

For only this figure, we ignore the redshift evolution of the correlation length and set  $r_0 = 4.8 h^{-1}$  Mpc. The expected mean number of companions per quasar with  $R < 50 h^{-1}$  kpc is  $\sim 2 - 3 \times 10^{-5}$  without incompleteness, so that in a sample of  $\sim 50,000$  quasars we expect to find roughly  $\sim 1$  quasar pair with separation  $< 50 h^{-1}$  kpc. However, our clustering sample already contains 20 quasars with transverse separations this small. Although our survey is far from complete, there is already evidence for excess clustering over what is expected from extrapolating the correlation function power law. In the next two sections we will make this argument more precise.

### 6.3. Computing the Selection Function

To estimate the correlation function, we will compute the total number of random pairs expected from eqn. (14) by summing over the redshifts of the quasars in each parent sample around which we searched around for candidate companions. However, we must first consider several sources of incompleteness. For the  $\chi^2$  selected sample, our  $\chi^2 < 20$  cut results in a completeness fraction,  $C(z, \chi^2 < 20)$ , shown in Figure 2. In addition, only a fraction of the pair candidates which satisfy the criteria for our lens and  $\chi^2$  selection algorithms have been observed to date, and the fraction of candidates observed varies with angular separation, because of our tendency to observe small separation pairs first. Finally, for the  $\theta > 60''$  pairs which we find in the SDSS spectroscopic sample, the completeness fraction is just that of the SDSS quasar survey and does not vary with angle.

The selection probability in eqn. (14) can therefore be written

$$S(z, \theta) = \begin{cases} F_{\text{lens}}(\theta) & \theta \leq 3'' \\ F_{\chi^2}(\theta) C(z | \chi^2 < 20) & 3'' < \theta \leq 60'' \\ F_{\text{spec}} & \theta > 60'' \end{cases} \quad (17)$$

where  $F_{\text{lens}}(\theta)$ ,  $F_{\chi^2}(\theta)$ , and  $F_{\text{spec}}$  are the completeness fractions of the lens,  $\chi^2$ , and spectroscopic samples, respectively.

We take  $F_{\text{spec}} = 0.95$  following Vanden Berk et al. (2005). The angular selection functions,  $F_{\text{lens}}(\theta)$  and  $F_{\chi^2}(\theta)$ , of the lens and  $\chi^2$  selection algorithms, are computed by comparing, in bins, the number of pair candidates which have been observed to date to the total number of candidates.

For  $\theta < 15''$ , we choose the bin spacing such that each bin contains at least 6 objects. For  $15'' < \theta < 60''$  we use ten logarithmically spaced angular bins.

The selection probability for the angular bin  $[\theta_k, \theta_{k+1}]$  is

$$F_k = \frac{N_{\text{observed}}}{N_{\text{observed}} + N_{\text{remaining}}}. \quad (18)$$

There is an uncertainty in the number of remaining candidates for the lens selection, which is based on the goodness of fit of a multi-component PSF to the images of SDSS quasars (Pindor et al. 2003; Inada et al. 2003). Because our observations were heavily biased towards those candidates which were likely to be quasar pairs, we bracket the angular selection function  $F_{\text{lens}}(\theta)$  with upper and lower limits corresponding to pessimistic and optimistic assessments of the number of remaining candidates which are likely to be confirmed as binaries. The lens candidates are given a grade of A, B, or C determined by the goodness of fit of the multi-component PSF. For the lower limit on  $F_{\text{lens}}(\theta)$ ,  $N_{\text{remaining}}$  is taken to be all candidates, whereas for the upper limit  $N_{\text{remaining}}$  is restricted to only the candidates which received a grade of A. Note that to be conservative, we have ignored the intrinsic incompleteness of the lens selection algorithm, which is a function of separation, magnitude, and flux ratio (Pindor et al. 2003) of the pair, and focus only on the incompleteness of our observations of the candidates.

The color-color diagrams of the candidates identified by  $\chi^2$  selection, were visually inspected prior to observations candidates which overlapped the stellar locus were given a lower priority. However, some interlopers were observed depending on a variety of criteria. For instance, we were more likely to observe pairs with particularly small angular separations, or redshifts  $z > 2$  (because of their use for Ly $\alpha$  forest studies), or those with particularly bright magnitudes. Including the stellar locus interlopers identified by the  $\chi^2$  statistic as part of  $N_{\text{remaining}}$  in eqn. (18) would overestimate the number of candidates likely to be quasar pairs and hence underestimate our selection function. To this end, we apply additional criteria to these remaining candidates to filter out color-matches which are likely to be quasar-star pairs. However, all quasar-star pairs we confirmed spectroscopically are included as part of  $N_{\text{observed}}$  in eqn. (18). In this way, we conservatively err on the side of overestimating our selection completeness, or underestimating the correlation function.

In addition to the criteria in eqn. (5), we only include  $\chi^2$  candidates which either (A) have colors consistent with the UV-excess region of color space ( $u-g < 0.6$ ) but outside the region populated by white dwarfs (Richards et al. 2002a), (B) matched a member of the faint photometric catalog of Richards et al. (2004) (extended to the DR3 region), or (C) were optically unresolved and matched a FIRST radio source. Objects that satisfy these criteria have a  $\gtrsim 90\%$  probability of being a quasar. For the UV-excess criteria, we conservatively required

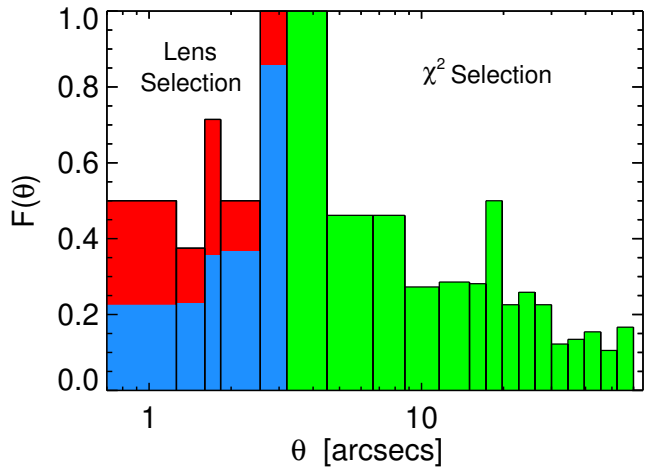


FIG. 10.— Angular selection function of binary quasars with  $\theta < 60''$ . We have pasted  $F_{\text{lens}}(\theta)$  and  $F_{\chi^2}(\theta)$  together at  $\theta = 3''$ . For  $\theta \leq 3''$ , the red and blue histograms represent, the upper and lower limits on the fraction of lens pair candidates observed to date, respectively. The green histogram shows the fraction of  $\chi^2$  pair candidates observed so far.

that the candidates'  $1\sigma$  photometric errors left it inside the UV-excess region and outside the white dwarf region.

The angular selection function of our binary quasar survey is shown in Figure 10.

#### 6.4. Excess Clustering

The individual quasar-random contributions for each selection algorithm were computed by carrying out the sum in eqn. (14) over the respective parent samples. Specifically, we summed over 39,142 quasars which were the parent sample for the lens sample, the 59,608 (SDSS+2QZ quasars) which were the parent sample of the  $\chi^2$  algorithm, and the 52,279 (SDSS only) quasars which made up the parent sample of the spectroscopic sample.

For the proper (comoving) projected correlation functions, we binned our clustering sample into 15 logarithmically spaced bins in the range  $9 h^{-1} \text{ kpc} < R_{\text{prop}} < 3 h^{-1} \text{ Mpc}$  ( $20 h^{-1} \text{ kpc} < R < 7 h^{-1} \text{ Mpc}$ ). Both projected correlation functions are compared to an extrapolation of the large scale power law measured by PMN in the left panels of Figures 11 and 12. The PMN correlation function is in comoving coordinates, which was translated to proper coordinates in each element of the average in eqn. (15). The error bars are one sigma Poisson counting errors, where we used the fitting formula in Gehrels (1986) for  $N < 30$ . The blue points show the measurement of the projected correlation function if we use the lower limit (optimistic) for the selection function of our lens algorithm (blue histogram in Figure 10) to predict the number of quasar-random pairs, while the black points use the upper limit. Uncertainty in our selection function changes only the innermost few bins, because our lens algorithm is restricted to angular separations  $\theta < 3''$ . These blue points are offset slightly to the right for the sake of illustration. The red rectangles indicate the prediction for the projected correlation function based on the large scale measurement of PMN,

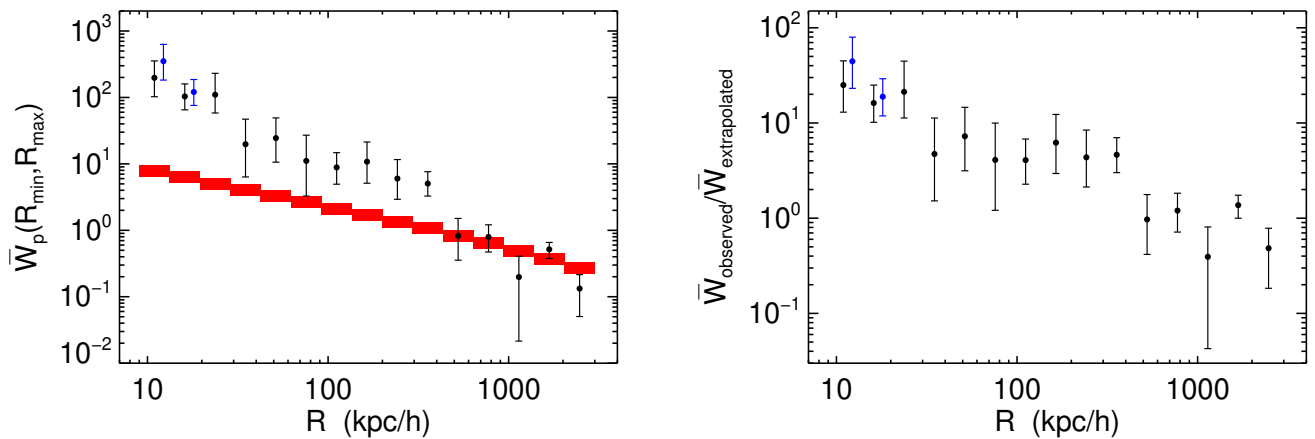


FIG. 11.— Small scale quasar clustering in proper coordinates *Left*: Comparison of the projected correlation function  $\bar{W}_p(R_{\min}, R_{\max}, z)$  (see eqn. 11) measured from our clustering sample with the prediction of the large scale measurement of PMN, extrapolated as a power law down to the scales probed by our binaries. Error bars are one sigma Poisson counting errors. The blue points show the measurement of the projected correlation function if we use the lower limit (optimistic) for the selection function of our lens algorithm (blue histogram in Figure 10) to predict the number of quasar-random pairs, rather than the upper limit, which are shown by the black points. The blue points are offset slightly to the right for the sake of illustration. Red rectangles indicate the prediction based on the large scale measurement of PMN, where the height of the rectangles indicate the range of predictions based on one sigma errors in the correlation length measurements, and the width indicate the bin used for each measurement. *Right* Ratio of the projected correlation function to the (best-fit) prediction of PMN.

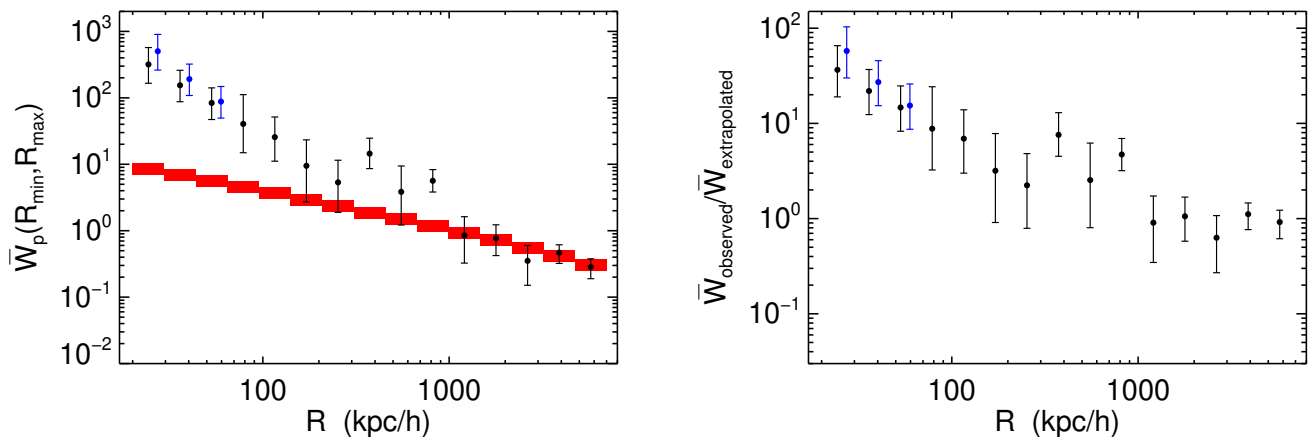


FIG. 12.— Same as Figure 11 except in comoving units.

extrapolated as a power law down to the scales probed by our sample. The heights of the rectangles are the range of predictions based on the one sigma errors on the correlation lengths (for each redshift interval) published by PMN, and the widths of the rectangles indicate the bin used for each measurement. The ratio of the measured projected correlation functions to the extrapolation of the best fit prediction of PMN are shown in the right panels of Figures 11 and 12.

A summary of the data plotted in these Figures is given in Tables 6 and 7. In the Tables we compare our calculation for the number of random pairs in each bin  $\langle QR \rangle$  (eqn. 14) for our survey to  $\langle QR \rangle_{\text{perfect}}$ , which is the expected number of random pairs for a ‘perfect’ survey with no sources of incompleteness. A comparison of these two quantities is a measure of our incompleteness in each bin.

Our clustering measurement agrees with the measurements of PMN for large proper (comoving) separations

$R_{\text{prop}} \gtrsim 400 h^{-1} \text{ kpc}$  ( $R \gtrsim 1 h^{-1} \text{ Mpc}$ ), where the PMN measurement is valid. However, we detect a significant excess over the expectation from extrapolating the power law of the correlation function to smaller scales. Although the uncertainties are large because of shot noise (and our uncertain selection function for  $\theta < 3''$ ), the excess is an order of magnitude for proper (comoving) separations  $R_{\text{prop}} \lesssim 40 h^{-1} \text{ kpc}$  ( $R \lesssim 100 h^{-1} \text{ kpc}$ ). The excess is largest ( $\sim 30$ ) on the smallest scales  $R_{\text{prop}} \sim 15 h^{-1} \text{ kpc}$  ( $R \sim 30 h^{-1} \text{ kpc}$ ).

Our clustering statistic  $W_p(R_{\min}, R_{\max})$  is the average over a cylinder shell with velocity extent  $4000 \text{ km s}^{-1}$ , corresponding to a typical extent  $r_{\text{prop}} \sim 18 h^{-1} \text{ Mpc}$  ( $r \sim r_0$ ) $^{-\gamma}$ ,  $W_p(R_{\min}, R_{\max})$  progressively flattens toward small scales, as is seen in red rectangles in the left panels of Figures 11 and 12. In contrast, our measured  $W_p(R_{\min}, R_{\max})$  does not flatten, but rather resembles a power law *in projection*. This necessarily implies that the

true three dimensional correlation function of quasars is not a power law  $\xi(r)$ , but rather gets *progressively steeper on small scales*.

## 7. DISCUSSION

On large proper comoving scales  $\gtrsim 1 h^{-1}$  Mpc, quasars at  $z \sim 1.5$ , similar to high redshift galaxies, are strongly biased, and have nearly the same correlation length that galaxies do in the local universe. In the previous section we argued that the correlation function of quasars becomes significantly *steeper* on sub-Mpc scales. Does small scale galaxy clustering or (quasar-galaxy clustering) show a similar trend? As we compare to previous clustering measurements in this section, all distances quoted are comoving.

At low redshift, Zehavi et al. (2004) measured the projected correlation function of the nearby ( $z \lesssim 0.2$ ) SDSS main galaxy sample ( $L \sim L^*$ ), down to scales as small as  $\sim 100 h^{-1}$  kpc. Eisenstein et al. (2005) measured the small scale clustering of Luminous Red Galaxies ( $L \sim 5 - 10L^*$ ) at intermediate redshift ( $0.2 \lesssim z \lesssim 0.3$ ), down to scales of  $\sim 300 h^{-1}$  kpc, by cross correlating them with  $L^*$  galaxies. Both of these studies find small deviations from a power law  $\gamma \sim -1.9$ , and the correlation function does steepen toward smaller scales. However, if these correlation function power laws were extrapolated from large ( $\sim 1 h^{-1}$  Mpc) scales to small, as we have done above for quasars, the clustering ‘excess’ would not be more than  $\sim 30\%$ . In comparison, we have found a much larger clustering excess, of a factor of  $\sim 7$  on scales  $R \sim 100 h^{-1}$  kpc and  $\sim 2 - 3$  on scales  $R \sim 300 h^{-1}$  kpc (see Table 7). One could argue that the proper comparison is with the square of the clustering excess measured by Eisenstein et al. (2005) (see discussion below), since it is a cross-correlation with less luminous galaxies. However Zehavi et al. (2005) measured the autocorrelation of LRGs at  $\sim 400 h^{-1}$  kpc, and also found an excess smaller than  $\sim 30\%$ .

Another complementary set of low redshift observations which probe clustering on small scales ( $10h^{-1}$  kpc– $1h^{-1}$  Mpc) are the SDSS galaxy-galaxy lensing studies (Guzik & Seljak 2002; Sheldon et al. 2004), which measure the galaxy-dark matter cross-correlation function. No excess small scale clustering over a power law was detected in these studies either.

A comparison with small scale galaxy clustering at high redshift is clearly more relevant to our purposes. Adelberger et al. (2003) and Coil et al. (2004) have measured the correlation function of galaxies at  $z \sim 3$  and  $z \sim 1$ , respectively, down to scales as small as  $\sim 100 - 200h^{-1}$  kpc, and no small scale excess clustering was found. As the redshift ranges of these measurements bracket the redshift range probed by our sample of binary quasars, we expect that galaxies in the redshift desert  $z \sim 1.4 - 2.5$ , coeval with the bulk of our binary quasars (see Figure 3), also do not show any enhancement in small scale clustering.

Thus, as first suggested by Djorgovski (1991), quasars at  $z \sim 1.5$  depart from the power law clustering hierarchy followed by galaxies, both in the local universe and at high redshift. Galaxy interactions are often implicated as a means of triggering, fueling, or forming active galactic nuclei (Toomre & Toomre 1972; Barnes & Hernquist 1996; Bahcall et al. 1997), and it has been claimed by

several authors that excess quasar clustering is the hallmark of these dissipative interaction events (Djorgovski 1991; Kochanek, Falco, & Muñoz 1999; Mortlock, Webster, & Francis 1999). However, if this is the case, a similar small scale enhancement is to be expected in the quasar-galaxy correlation function, as follows.

If the quasar-quasar correlation function is  $\xi_{QQ}$ , and quasars trace galaxy overdensities with a linear relative bias  $b_Q$  defined by  $\delta_Q = b_Q \delta_G$ , then the ratio of the quasar-quasar correlation to the galaxy-galaxy correlation is  $\xi_{QQ}/\xi_{GG} = b_Q^2$ , and the ratio of the quasar-galaxy cross correlation function to galaxy-galaxy clustering is  $\xi_{QG}/\xi_{GG} = b_Q$ . Since we have argued that small scale quasar clustering is enhanced relative to galaxy clustering at the same redshift, we expect to see the square root of that enhancement in the quasar-galaxy cross correlation.

It has long been known that quasars are associated with enhancements in the distribution of galaxies (Bahcall, Schmidt, & Gunn 1969; Yee & Green 1984, 1987; Bahcall & Chokshi 1991; Laurikainen & Salo 1995; Smith, Boyle, & Maddox 1995; Hall, Green, & Cohen 1998; Hall & Green 1998; Smith, Boyle, & Maddox 2000), and the foregoing argument has led us to ask if there is a small scale excess of galaxy pairs around quasars. However, nearly all studies of quasar-galaxy correlations have been restricted to low redshifts ( $z \lesssim 0.6$ ) and therefore low-luminosity, and the only correlation function measurements that probed the redshift range  $1 \lesssim z \lesssim 3$  relevant for comparison to our sample of binaries measured a marginal cross-correlation of quasars with galaxies (Teplitz, McLean, & Malkan 1999), or none at all (Boyle & Couch 1993; Croom & Shanks 1999; Infante et al. 2003). We note that the disagreement in the literature on whether radio-loud quasars are located in richer environments (Yee & Green 1984, 1987; Ellingson, Yee, & Green 1991) or not (Fisher et al. 1996; McLure & Dunlop 2001; Finn, Impey, & Hooper 2001; Wold et al. 2001), is not an issue in the current context, since only one close binary in our clustering sub-sample, LBQS1429–008, has a radio loud member.

Historically, there has been significant scatter in the low redshift measurements of quasar-galaxy correlations (see Brown, Boyle, & Webster 2001, Table 1 for a compilation of recent studies) caused by heterogeneous quasar samples, methodology, and imaging depths. Furthermore, the measurement of a factor of  $\sim 4$  enhancement of the number of companion galaxies around quasars compared to the mean number around galaxies, measured by the Hubble Space Telescope Studies of  $\sim 40$  nearby AGN by Fisher et al. (1996) and McLure & Dunlop (2001), has been called into question by Finn, Impey, & Hooper (2001) as being the result of sample biases. We thus focus on the most recent determinations of quasar galaxy correlations, albeit at low redshifts  $z \lesssim 0.3$ , by the 2dF and SDSS; these surveys have samples of  $\sim 10,000$  AGN surrounded by  $\sim 100,000$  galaxies at their disposal.

Croom et al. (2004a) and Wake et al. (2004) measured the ratio  $\xi_{QG}/\xi_{GG} = b_Q$ , in the 2dF and SDSS surveys respectively, finding it to be consistent with unity on small and large scales. The Croom et al. (2004a) measurement extends down to  $\sim 900 h^{-1}$  kpc; whereas the Wake et al. (2004) measurement probes down to scales  $\sim$

TABLE 6  
 PROJECTED CORRELATION FUNCTION IN PROPER COORDINATES

$R_{\min}$	$R_{\max}$	$\langle QQ \rangle$	$\langle QR \rangle$	$\langle QR \rangle_{\text{perfect}}$	$\bar{W}_p$	$\bar{W}_p^{\text{PMN}}$	Ratio
9.00	13.26	4	0.02014 (0.01136)	0.03147	197.60 (350.98)	7.89	25.0 (44.5)
13.26	19.53	7	0.06694 (0.05749)	0.06922	103.57 (120.76)	6.40	16.2 (18.9)
19.53	28.76	5	0.04506	0.2240	109.96	5.17	21.3
28.76	42.37	2	0.09635	0.4860	19.76	4.18	4.73
42.37	62.40	3	0.11784	1.055	24.46	3.37	7.26
62.40	91.92	2	0.1654	2.288	11.09	2.71	4.09
91.92	135.39	6	0.6090	4.964	8.85	2.17	4.07
135.39	199.42	7	0.5938	10.77	10.79	1.74	6.22
199.42	293.74	8	1.142	23.37	6.01	1.38	4.36
293.74	432.67	20	3.305	37.30	5.05	1.09	4.64
432.67	637.31	23	12.59	13.25	0.83	0.85	0.97
637.31	938.74	49	27.31	28.75	0.79	0.66	1.20
938.74	1382.73	71	59.26	62.38	0.20	0.50	0.39
1382.73	2036.71	195	128.6	135.3	0.52	0.38	1.37
2036.71	3000.00	316	279.0	293.6	0.13	0.27	0.48

NOTE. — Data for clustering measurements shown in Figure 11. The 15 logarithmically spaced bins of proper transverse separation are given by  $R_{\min}$  and  $R_{\max}$  in  $h^{-1}$  kpc. The number of observed pairs in our clustering sub-sample for each bin is given by  $\langle QQ \rangle$ . Our calculation of the number of random pairs in each bin is  $\langle QR \rangle$  (eqn. 14), and  $\langle QR \rangle_{\text{perfect}}$  is the expected number of random pairs for a ‘perfect’ survey with no sources of incompleteness. Our measurement of the projected correlation function is given by  $\bar{W}_p(R_{\min}, R_{\max})$ . The quantity  $\bar{W}_p^{\text{PMN}}(R_{\min}, R_{\max})$  is the prediction from the larger scale clustering measurements of PMN, extrapolated as a power law down to the scale probed by our binaries, and averaged over the redshift distribution of our parent quasar sample (see eqn. 15). The ratio of our measurement to the prediction from PMN is given in the last column. The quantities in parentheses are the measurements if we use the lower limit for the selection function of the ‘lens’ algorithm (blue histogram in Figure 10) to predict  $\langle QR \rangle$ , which corresponds to the blue points in Figure 11.

 TABLE 7  
 PROJECTED CORRELATION FUNCTION IN COMOVING COORDINATES

$R_{\min}$	$R_{\max}$	$\langle QQ \rangle$	$\langle QR \rangle$	$\langle QR \rangle_{\text{perfect}}$	$\bar{W}_p$	$\bar{W}_p^{\text{PMN}}$	Ratio
20.00	29.56	4	0.01251 (0.007935)	0.02452	318.69 (503.12)	8.73	36.5 (57.6)
29.56	43.68	5	0.03213 (0.02595)	0.06007	154.61 (191.66)	7.06	21.9 (27.1)
43.68	64.54	5	0.05895 (0.05623)	0.1674	83.81 (87.92)	5.71	14.7 (15.4)
64.54	95.38	3	0.07226	0.3886	40.52	4.61	8.80
95.38	140.95	3	0.1127	0.8487	25.63	3.71	6.91
140.95	208.28	2	0.1907	1.853	9.49	2.98	3.18
208.28	307.80	3	0.4731	4.047	5.34	2.39	2.24
307.80	454.85	10	0.6467	8.839	14.46	1.91	7.58
454.85	672.16	5	1.032	18.75	3.85	1.52	2.54
672.16	993.29	21	3.160	29.00	5.65	1.20	4.71
993.29	1467.84	20	10.80	13.29	0.85	0.94	0.91
1467.84	2169.12	42	23.71	24.96	0.77	0.73	1.06
2169.12	3205.45	70	51.78	54.51	0.35	0.56	0.63
3205.45	4736.89	166	113.1	119.0	0.47	0.42	1.11
4736.89	7000.00	317	246.9	259.9	0.28	0.31	0.92

NOTE. — Same as Table 6 except in comoving coordinates (Figure 12).

$400h^{-1}$  kpc. Both of these studies cross-correlated spectroscopic samples of galaxies with spectroscopic samples of AGN; hence, they are limited to low redshift  $z \lesssim 0.3$ , because the spectroscopic galaxy samples are shallow, and large scales, because of fiber collisions. At  $z \sim 0.2$  the fiber collision limit corresponds to  $\sim 160 h^{-1}$  kpc in the SDSS and  $\sim 80 h^{-1}$  kpc in the 2dF. What is needed is a clustering study using photometric galaxies around spectroscopic quasars which could extend to redshift  $z \sim 0.5$  and resolve the scales  $R \sim 10 h^{-1}$  kpc of most interest to us for the excess quasar clustering (see Serber et al. 2004, in preparation).

## 8. SUMMARY AND CONCLUSIONS

We have presented a sample of 218 new quasar pairs with transverse separations  $R_{\text{prop}} < 1 h^{-1}$  Mpc over the redshift range  $0.5 \leq z \leq 3.0$ . Of these, 65 have angular separations  $\theta < 60''$  below the SDSS fiber collision scale. Our 26 new pairs with proper separations  $R_{\text{prop}} < 50 h^{-1}$  kpc ( $\theta < 10''$ ) more than doubles the number of binaries known with splittings this small. Although these binaries were discovered with a variety of selection algorithms, we defined a statistical sub-sample selected with homogeneous criteria, and computed its selection function taking into account sources of incompleteness. We presented the first measurement of the quasar correlation function on the small proper (comoving) scales  $10 h^{-1}$  kpc –  $400 h^{-1}$  kpc ( $20 h^{-1}$  kpc –  $1 h^{-1}$  Mpc). We detect an order of magnitude excess clustering for

proper (comoving) separations  $R_{\text{prop}} \lesssim 40 h^{-1}$  kpc ( $R \lesssim 100 h^{-1}$  kpc), which grows to  $\sim 30$  on the smallest scale probed by our sample,  $R_{\text{prop}} \sim 15 h^{-1}$  kpc ( $R \sim 30 h^{-1}$  kpc).

We reviewed recent small scale measurements of galaxy clustering and quasar-galaxy clustering and discussed the results in relation to the excess small scale quasar clustering that we measured. The quasar-galaxy correlation function of redshift  $z \sim 1.5$  quasars should show a small scale clustering enhancement with amplitude roughly the square root of the enhancement detected here. However, existing studies of the environments of quasars at  $z \sim 1.5$  have been plagued by small sample sizes and lack the statistics to address the clustering strength on the  $\sim 100 h^{-1}$  kpc scales of interest.

Deep imaging of the binaries published here will provide valuable information about their environments. The detection of significant overdensities of galaxies coeval with the binary would support the idea that enhanced quasar activity is triggered by galaxy interactions, and it might suggest that quasars at high redshift trace the biased peaks which are the progenitors of the rich clusters we see today (Efstathiou & Rees 1988; Cole & Kaiser 1989; Nusser & Silk 1993; Djorgovski et al. 1999; Djorgovski 1999; Djorgovski et al. 2003). Intriguingly, Fukugita et al. (2004) took deep Subaru images of the  $z = 4.25$  quasar discovered by Schneider et al. (2000), and found no evidence for an overdensity of galaxies. Similar deep imaging studies of high redshift quasar environments (for single quasars) have been conducted by Infante et al. (2003) at  $z \sim 3$ , and by Djorgovski and collaborators at  $z \gtrsim 4$  (Djorgovski et al. 1999; Djorgovski 1999; Djorgovski et al. 2003; Stiavelli et al. 2005). The binaries in our sample offer an opportunity to conduct analogous studies over a range of lower and more accessible redshifts, with the added bonus that one expects these extremely rare binary systems to trace even richer environments.

Measurements of the shape of the quasar-quasar and quasar-galaxy correlation function on the small scales probed by our binaries will yield valuable insights into the physical processes that trigger quasar activity and will help explain how quasars are embedded in the structure formation hierarchy. Reproducing the excess clustering with semi-analytical models (Kauffmann & Haehnelt 2002) and halo models (see e.g. PMN) would provide constraints on the distribution of quasars in dark matter halos. Another interesting question is whether the quasars in these binaries have significantly longer lifetimes than ‘field’ quasars (Haiman & Hui 2001; Martini & Weinberg 2001), which would have interesting implications for the masses of supermassive black holes (Wyithe & Loeb 2004) in the richest regions of the Universe.

We close with the reminder that our survey for quasar pairs is ongoing and less than 50% complete. We expect to find a comparable number of binaries in the current SDSS quasar sample. Furthermore, the faint photometric quasar selection techniques of Richards et al. (2004) aim to construct a sample of  $\sim 10^6$  quasars. Extrapolating from the number of pairs published here, we would expect to find  $\sim 1000$  new binaries in a sample of this size, which would allow a much more precise measurement of the correlation function on small scales.

JFH wishes to thank his thesis advisor David Spergel for advice, guidance, and helpful discussions over the course of this work during his time in Princeton. For part of this study JFH was supported by the Proctor Graduate fellowship at Princeton University and by a generous gift from the Paul & Daisy Soros Fellowship for New Americans. The program is not responsible for the views expressed. JFH is currently supported by NASA through Hubble Fellowship grant # 01172.01-A awarded by the Space Telescope Science Institute, which is operated by the Association of Universities for Research in Astronomy, Inc., for NASA, under contract NAS 5-26555. Thanks to Bob Nichol and Alex Gray for help with the faint photometric quasar catalog. We are grateful to the observing specialists at Apache Point Observatory, Russet MacMillan, John Barentine, Bill Ketzbeck, and Jack Dembicky for many nights of hard work.

Funding for the creation and distribution of the SDSS Archive has been provided by the Alfred P. Sloan Foundation, the Participating Institutions, the National Aeronautics and Space Administration, the National Science Foundation, the U.S. Department of Energy, the Japanese Monbukagakusho, and the Max Planck Society. The SDSS Web site is <http://www.sdss.org/>. The SDSS is managed by the Astrophysical Research Consortium (ARC) for the Participating Institutions. The Participating Institutions are The University of Chicago, Fermilab, the Institute for Advanced Study, the Japan Participation Group, The Johns Hopkins University, the Korean Scientist Group, Los Alamos National Laboratory, the Max-Planck-Institute for Astronomy (MPIA), the Max-Planck-Institute for Astrophysics (MPA), New Mexico State University, University of Pittsburgh, University of Portsmouth, Princeton University, the United States Naval Observatory, and the University of Washington.

This paper is based in part on data collected at the W. M. Keck Observatory, the Apache Point Observatory 3.5m Telescope, the Hobby-Eberly Telescope, and the European Southern Observatory, Chile, (proposal #67.A-0544). The Apache Point Observatory (APO) 3.5-meter telescope, is owned and operated by the Astrophysical Research Consortium. The W. M. Keck Observatory is operated as a scientific partnership among the California Institute of Technology, the University of California, and the National Aeronautics and Space Administration. The Hobby-Eberly Telescope (HET) is a joint project of the University of Texas at Austin, the Pennsylvania State University, Stanford University, Ludwig-Maximilians-Universität München, and Georg-August-Universität Göttingen. The HET is named in honor of its principal benefactors, William P. Hobby and Robert E. Eberly. The Marcario Low-Resolution Spectrograph is named for Mike Marcario of High Lonesome Optics, who fabricated several optics for the instrument but died before its completion; it is a joint project of the Hobby-Eberly Telescope partnership and the Instituto de Astronomía de la Universidad Nacional Autónoma de México.

DPS acknowledges support from NSF grant (AST03-07582) and MAS acknowledges the support of NSF grant (AST-0307409).

A portion of this work was also performed under the auspices of the U.S. Department of Energy, National Nu-



TABLE 1  
 PROJECTED PAIRS OF QUASARS DISCOVERED IN OVERLAPPING PLATES

Name	RA	Dec	$u$	$g$	$r$	$i$	$z$	$z$	$\Delta\theta$	$R_{\text{prop}}$
SDSSJ0000+0055A	00:00:42.91	+00:55:39.5	18.30	18.16	17.99	18.01	17.88	0.95	170.7	961.9
SDSSJ0000+0055B	00:00:42.91	+00:55:39.5	20.01	19.69	19.44	19.39	19.43	1.18		
SDSSJ0004+0000A	00:04:42.18	+00:00:23.4	19.24	19.09	18.85	18.95	19.07	1.01	134.0	626.4
SDSSJ0004+0001B	00:04:42.18	+00:00:23.4	20.91	20.39	20.22	19.83	19.52	0.58		

NOTE. — Quasars labeled SDSS or 2QZ are members of the SDSS or 2QZ spectroscopic quasar catalog. The redshift of each quasar is indicated by the column  $z$  and the foreground quasar is always designated ‘A’. The column labeled  $R_{\text{prop}}$  is the transverse proper separation at the foreground quasar in  $h^{-1}$  kpc, extinction corrected SDSS five band PSF photometry is given in the columns  $u$ ,  $g$ ,  $r$ ,  $i$ , and  $z$ , and  $\Delta\theta$  is the angular separation in arcseconds

 TABLE 2  
 PROJECTED PAIRS OF QUASARS DISCOVERED FROM FOLLOW UP SPECTROSCOPY

Name	RA	Dec	$u$	$g$	$r$	$i$	$z$	$z$	$\Delta\theta$	$R$	$\chi^2$
APOJ0002+0053A	00:02:12.53	−00:53:11.7	20.72	20.59	20.34	20.12	20.17	1.54	7.3	44.5	20.9
SDSSJ0002+0053B	00:02:12.53	−00:53:11.7	20.10	19.64	19.52	19.41	19.23	2.21			
SDSSJ0036+1109A	00:36:49.63	−11:09:29.8	19.08	18.85	18.67	18.45	18.67	1.51	4.7	28.5	19.0
APOJ0036+1109B	00:36:49.63	−11:09:29.8	20.92	20.64	20.46	20.52	20.24	2.18			

NOTE. — Quasars labeled SDSS or 2QZ are members of the SDSS or 2QZ spectroscopic quasar catalog. Quasars discovered from follow up spectroscopy are labeled APO. The redshift of each quasar is indicated by the column  $z$  and the foreground quasar is always designated ‘A’. The column labeled  $R_{\text{prop}}$  is the transverse proper separation at the foreground quasar in  $h^{-1}$  kpc, extinction corrected SDSS five band PSF photometry is given in the columns  $u$ ,  $g$ ,  $r$ ,  $i$ , and  $z$ ,  $\Delta\theta$  is the angular separation in arcseconds, and  $\chi^2$  is the value of our color similarity statistic.

 TABLE 3  
 QUASAR-STAR PAIRS DISCOVERED FROM FOLLOW UP SPECTROSCOPY<sup>†</sup>

Name	RA	Dec	$u$	$g$	$r$	$i$	$z$	$z$	$\Delta\theta$	$\chi^2$
SDSSJ0006+0026A	00:06:14.00	+00:26:05.0	20.85	20.09	19.98	19.95	19.81	2.51	28.0	42.4
APOJ0006+0026B	00:06:14.00	+00:26:05.0	21.04	20.16	19.83	19.70	19.78			
SDSSJ0015+0048A	00:15:57.08	+00:48:22.4	20.74	19.95	19.63	19.57	19.29	2.31	53.5	5.4
APOJ0015+0048B	00:15:57.08	+00:48:22.4	21.12	20.38	20.08	19.96	19.87			

NOTE. — Quasars labeled SDSS or 2QZ are members of the SDSS or 2QZ spectroscopic quasar catalog and are always designated by ‘A’. Stars discovered from follow up spectroscopy are labeled APO and designated by ‘B’. The redshift of the quasar is indicated by the column  $z$ , extinction corrected SDSS five band PSF photometry is given in the columns  $u$ ,  $g$ ,  $r$ ,  $i$ , and  $z$ ,  $\Delta\theta$  is the angular separation in arcseconds, and  $\chi^2$  is the value of our color similarity statistic.

clear Security Administration by the University of California, Lawrence Livermore National Laboratory under

contract No. W-7405-Eng-48.

## APPENDIX

In this appendix we present the results of all of our follow up observations not included above, as well as list of projected pairs of quasars in the SDSS quasar sample which have similar redshifts. These tables will facilitate future studies of close quasar pairs and prevent the duplicate observations of candidates already observed by the SDSS or our follow up observation program.

In Table 1 we list all projected pairs of quasars in the combined SDSS+2QZ spectroscopic catalog with proper transverse separations  $R_{\text{prop}} < 1 h^{-1}$  Mpc at the foreground quasar and redshift difference  $\Delta z < 0.5$ . All projected pairs of quasars discovered from our follow up spectroscopic observations are listed in Table 2. Finally, Table 3 lists all of the quasar-star pairs identified from our follow up observations. The full versions of these tables are published in in the electronic version of this article.

## REFERENCES

- Abazajian, K., et al. 2003, AJ, 126, 2081  
 Abazajian, K., et al. 2004, AJ, 128, 502  
 Abazajian, K., et al. 2005, AJ, 129, 1755  
 Adelberger, K. L., Steidel, C. C., Shapley, A. E., & Pettini, M. 2003, ApJ, 584, 45  
 Alcock, C. & Paczynski, B. 1979, Nature, 281, 358  
 Anderson, S. F., et al. 2003, AJ, 126, 2209  
 Andreani, P. & Cristiani, S. 1992, ApJ, 398, L13  
 Bahcall, J. N., Kirhakos, S., Saxe, D. H., & Schneider, D. P. 1997, ApJ, 479, 642

- 21
- Bahcall, J. N., Schmidt, M., & Gunn, J. E. 1969, *ApJ*, 157, L77
- Bahcall, N. A. & Chokshi, A. 1991, *ApJ*, 380, L9
- Barnes, J. E. & Hernquist, L. 1996, *ApJ*, 471, 115
- Becker, R. H., White, R. L., & Helfand, D. J. 1995, *ApJ*, 450, 559
- Blanton, M. R., Lin, H., Lupton, R. H., Maley, F. M., Young, N., Zehavi, I., & Loveday, J. 2003, *AJ*, 125, 2276
- Bonnet, H., Fort, B., Kneib, J.-P., Mellier, Y., & Soucail, G. 1993, *A&A*, 280, L7
- Boyle, B. J. & Couch, W. J. 1993, *MNRAS*, 264, 604
- Boyle, B. J., Shanks, T., Croom, S. M., Smith, R. J., Miller, L., Loaring, N., & Heymans, C. 2000, *MNRAS*, 317, 1014
- Brown, M. J. I., Boyle, B. J., & Webster, R. L. 2001, *AJ*, 122, 26
- Budavári, T., et al. 2001, *AJ*, 122, 1163
- Cao, L., Wei, J.-Y., & Hu, J.-Y. 1999, *A&AS*, 135, 243
- Carlberg, R. G. 1990, *ApJ*, 350, 505
- Castander, F. J., et al. 2001, *AJ*, 121, 2331
- Coil, A. L., et al. 2004, *ApJ*, 609, 525
- Cole, S. & Kaiser, N. 1989, *MNRAS*, 237, 1127
- Colley, W. N., Tyson, J. A., & Turner, E. L. 1996, *ApJ*, 461, L83
- Crampton, D., Cowley, A. P., Hickson, P., Kindl, E., Wagner, R. M., Tyson, J. A., & Gullixson, C. 1988, *ApJ*, 330, 184
- Croom, S. M., Boyle, B. J., Loaring, N. S., Miller, L., Outram, P. J., Shanks, T., & Smith, R. J. 2002, *MNRAS*, 335, 459
- Croom, S. M. & Shanks, T. 1996, *MNRAS*, 281, 893
- Croom, S. M. & Shanks, T. 1999, *MNRAS*, 303, 411
- Croom, S. M., Shanks, T., Boyle, B. J., Smith, R. J., Miller, L., Loaring, N. S., & Hoyle, F. 2001, *MNRAS*, 325, 483
- Croom, S., et al. 2004a, *AGN Physics with the Sloan Digital Sky Survey*, edited by G.T. Richards and P. B. Hall, ASP Conference Series 311, 457
- Croom, S. M., Smith, R. J., Boyle, B. J., Shanks, T., Miller, L., Outram, P. J., & Loaring, N. S. 2004b, *MNRAS*, 349, 1397
- Croom, S. M., et al. 2005, *MNRAS*, 356, 415
- Djorgovski, S. 1991, ASP Conf. Ser. 21: The Space Distribution of Quasars, 349
- Djorgovski, S. G. 1999, ASP Conf. Ser. 193: The Hy-Redshift Universe: Galaxy Formation and Evolution at High Redshift, 397
- Djorgovski, S. G., Odewahn, S. C., Gal, R. R., Brunner, R. J., & de Carvalho, R. R. 1999, ASP Conf. Ser. 191: Photometric Redshifts and the Detection of High Redshift Galaxies, 179
- Djorgovski, S. G., Stern, D., Mahabal, A. A., & Brunner, R. 2003, *ApJ*, 596, 67
- Dobrzycki, A. & Bechtold, J. 1991, *ApJ*, 377, L69
- Duncan, R. C. 1991, *ApJ*, 375, L41
- Efstathiou, G. & Rees, M. J. 1988, *MNRAS*, 230, 5P
- Eisenstein, D. J., et al. 2001, *AJ*, 122, 2267
- Eisenstein, D. J., Blanton, M., Zehavi, I., Bahcall, N., Brinkmann, J., Loveday, J., Meiksin, A., & Schneider, D. 2005, *ApJ*, 619, 178
- Ellingson, E., Yee, H. K. C., & Green, R. F. 1991, *ApJ*, 371, 49
- Epps, H. W. & Miller, J. S. 1998, *Proc. SPIE*, 3355, 48
- Fan, X., et al. 1999, *AJ*, 118, 1
- Fan, X., et al. 2001, *AJ*, 121, 54
- Fernandez-Soto, A., Barcons, X., Carballo, R., & Webb, J. K. 1995, *MNRAS*, 277, 235
- Ferrarese, L. & Merritt, D. 2000, *ApJ*, 539, L9
- Finn, R. A., Impey, C. D., & Hooper, E. J. 2001, *ApJ*, 557, 578
- Fischer, P., Tyson, J. A., Bernstein, G. M., & Guhathakurta, P. 1994, *ApJ*, 431, L71
- Fisher, K. B., Bahcall, J. N., Kirhakos, S., & Schneider, D. P. 1996, *ApJ*, 468, 469
- Fukugita, M., Ichikawa, T., Gunn, J. E., Doi, M., Shimasaku, K., & Schneider, D. P. 1996, *AJ*, 111, 1748
- Fukugita, M., Nakamura, O., Schneider, D. P., Doi, M., & Kashikawa, N. 2004, *ApJ*, 603, L65
- Gebhardt, K., et al. 2000, *ApJ*, 539, L13
- Gehrels, N. 1986, *ApJ*, 303, 336
- Gnedin, N. Y. & Hui, L. 1998, *MNRAS*, 296, 44
- Green, P. J., et al. 2002, *ApJ*, 571, 721
- Gregg, M. D., Becker, R. H., White, R. L., Richards, G. T., Chaffee, F. H., & Fan, X. 2002, *ApJ*, 573, L85
- Gunn, J. E., et al. 1998, *AJ*, 116, 3040
- Guzik, J. & Seljak, U. 2002, *MNRAS*, 335, 311
- Haehnelt, M. G. & Rees, M. J. 1993, *MNRAS*, 263, 168
- Hagen, H.-J., Hopp, U., Engels, D., & Reimers, D. 1996, *A&A*, 308, L25
- Haiman, Z. & Hui, L. 2001, *ApJ*, 547, 27
- Hall, P. B., & Green, R. F. 1998, *ApJ*, 507, 558
- Hall, P. B., Green, R. F., & Cohen, M. 1998, *ApJS*, 119, 1
- Hawkins, M. R. S., Clements, D., Fried, J. W., Heavens, A. F., Veron, P., Minty, E. M., & van der Werf, P. 1997, *MNRAS*, 291, 811
- Heckman, T. M., Armus, L., & Miley, G. K. 1990, *ApJS*, 74, 833
- Hennawi, J. F., Dalal, N., & Bode, P. 2005a, in preparation
- Hennawi, J. F. et al. 2005b, in preparation
- Hewett, P. C., Webster, R. L., Harding, M. E., Jedrzejewski, R. J., Foltz, C. B., Chaffee, F. H., Irwin, M. J., & Le Fevre, O. 1989, *ApJ*, 346, L61
- Hewett, P. C., Foltz, C. B., Harding, M. E., & Lewis, G. F. 1998, *AJ*, 115, 383
- Hill, G. J., Nicklas, H. E., MacQueen, P. J., Mitsch, W., Wellem, W., Altmann, W., Wesley, G. L., & Ray, F. B. 1998, *Proc. SPIE*, 3355, 433
- Hogg, D. W., Finkbeiner, D. P., Schlegel, D. J., & Gunn, J. E. 2001, *AJ*, 122, 2129
- Hogg, D. W., Baldry, I. K., Blanton, M. R., Eisenstein, D. J. 2002, ArXiv Astrophysics e-prints, astro-ph/0210394
- Hogan, C. & Narayan, R. 1984, *MNRAS*, 211, 575
- Hopkins, P. F., et al. 2004, *AJ*, 128, 1112
- Hui, L. & Haiman, Z. 2003, *ApJ*, 596, 9
- Hui, L., Stebbins, A., & Burles, S. 1999, *ApJ*, 511, L5
- Inada, N., et al. 2003a, *AJ*, 126, 666
- Inada, N., et al. 2003b, *Nature*, 426, 810
- Infante, L., Varela, J., Moles, M., Hertling, G., García, A., & Menanteau, F. 2003, *ApJ*, 588, 90
- Iovino, A. & Shaver, P. A. 1988, *ApJ*, 330, L13
- Kaiser, N. 1984, *ApJ*, 284, L9
- Kashikawa, N., et al. 2002, *PASJ*, 54, 819
- Kauffmann, G. & Haehnelt, M. G. 2002, *MNRAS*, 332, 529
- Kochanek, C. S., Falco, E. E., & Muñoz, J. A. 1999, *ApJ*, 510, 590
- Kochanek, C. S. et al. CASTLES Survey. at <http://cfa-www.harvard.edu/castles/> (2003).
- Koopmans, L. V. E., et al. 2000, *A&A*, 361, 815
- Kruszewski, A. 1988, *Acta Astronomica*, 38, 155
- Kundic, T. 1997, *ApJ*, 482, 631
- Lacey, C. & Cole, S. 1993, *MNRAS*, 262, 627
- Laurikainen, E. & Salo, H. 1995, *A&A*, 293, 683
- Lidz, A., Hui, L., Crofts, A. P. S., & Zaldarriaga, M. 2003, ArXiv Astrophysics e-prints, astro-ph/0309204
- Lupton, R. H., Gunn, J. E., & Szalay, A. S. 1999, *AJ*, 118, 1406
- Lupton, R. H., Gunn, J. E., Ivezić, Z., Knapp, G. R., Kent, S., & Yasuda, N. 2001, ASP Conf. Ser. 238: Astronomical Data Analysis Software and Systems X, 10, 269
- Madau, P., Haardt, F., & Rees, M. J. 1999, *ApJ*, 514, 648
- Magorrian, J., et al. 1998, *AJ*, 115, 2285
- Maoz, D., Rix, H., Gal-Yam, A., & Gould, A. 1997, *ApJ*, 486, 75
- Marble, A. R., Impey, C. D., Miller, L., Clewley, L., Edmondson, E., & Lopes, A. M. 2004, American Astronomical Society Meeting Abstracts, 205,
- Malhotra, S., Rhoads, J. E., & Turner, E. L. 1997, *MNRAS*, 288, 138
- Martini, P. & Weinberg, D. H. 2001, *ApJ*, 547, 12
- McDonald, P. 2003, *ApJ*, 585, 34
- McDonald, P. & Miralda-Escudé, J. 1999, *ApJ*, 518, 24
- McDonald, P., Miralda-Escudé, J., Rauch, M., Sargent, W. L. W., Barlow, T. A., Cen, R., & Ostriker, J. P. 2000, *ApJ*, 543, 1
- McDonald, P., et al. 2004, ArXiv Astrophysics e-prints, astro-ph/0405013
- McLure, R. J. & Dunlop, J. S. 2001, *MNRAS*, 321, 515
- Meylan, G., & Djorgovski, S. 1989, *ApJ*, 338, L1
- Miller, L., Lopes, A. M., Smith, R. J., Croom, S. M., Boyle, B. J., Shanks, T., & Outram, P. 2004, *MNRAS*, 348, 395
- Miyazaki, S., et al. 2002, *PASJ*, 54, 833
- Moller, P. & Kjaergaard, P. 1992, *A&A*, 258, 234
- Mo, H. J. & Fang, L. Z. 1993, *ApJ*, 410, 493
- Mortlock, D. J., Webster, R. L., & Francis, P. J. 1999, *MNRAS*, 309, 836
- Nusser, A. & Silk, J. 1993, *ApJ*, 411, L1
- Ofek, E. O., Maoz, D., Prada, F., Kolatt, T., & Rix, H. 2001, *MNRAS*, 324, 463
- Oguri, M., & Keeton, C. R. 2004, *ApJ*, 610, 663
- Oguri, M., et al. 2004, *ApJ*, 605, 78
- Oguri, M., et al. 2005, *ApJ*, 622, 106
- Oke, J. B. 1990, *AJ*, 99, 1621
- Oke, J. B. & Gunn, J. E. 1983, *ApJ*, 266, 713
- Oke, J. B., et al. 1995, *PASP*, 107, 375

- Osmer, P. S. 1981, *ApJ*, 247, 762
- Paczynski, B. 1986, *Nature*, 319, 567
- Patton, D. R., Carlberg, R. G., Marzke, R. O., Pritchett, C. J., da Costa, L. N., & Pellegrini, P. S. 2000, *ApJ*, 536, 153
- Pello, R., Miralles, J. M., Le Borgne, J.-F., Picat, J.-P., Soucail, G., & Bruzual, G. 1996, *A&A*, 314, 73
- Peng, C. Y., et al. 1999, *ApJ*, 524, 572
- Phillips, P. M., et al. 2001, *MNRAS*, 328, 1001
- Phinney, E. S. & Blandford, R. D. 1986, *Nature*, 321, 569
- Pier, J. R., Munn, J. A., Hindsley, R. B., Hennessy, G. S., Kent, S. M., Lupton, R. H., & Ivezić, Ž. 2003, *AJ*, 125, 1559
- Pindor, B., Turner, E. L., Lupton, R. H., & Brinkmann, J. 2003, *AJ*, 125, 2325
- Pindor, B., et al. 2005, *ApJ*, submitted
- Porciani, C. & Giavalisco, M. 2002, *ApJ*, 565, 24
- Porciani, C., Magliocchetti, M., & Norberg, P. [PMN] 2004, *ArXiv Astrophysics e-prints*, astro-ph/0406036
- Rauch, M., Sargent, W. L. W., Barlow, T. A., & Carswell, R. F. 2001, *ApJ*, 562, 76
- Richards, G. T., et al. 2001a, *AJ*, 121, 2308
- Richards, G. T., et al. 2001b, *AJ*, 122, 1151
- Richards, G. T., et al. 2002a, *AJ*, 123, 2945
- Richards, G. T., Vanden Berk, D. E., Reichard, T. A., Hall, P. B., Schneider, D. P., SubbaRao, M., Thakar, A. R., & York, D. G. 2002b, *AJ*, 124, 1
- Richards, G. T., et al. 2003, *AJ*, 126, 1131
- Richards, G. T., et al. 2004, *ApJS*, 155, 257
- Richards, G. T., et al. 2005, *MNRAS*, in press (astro-ph/0504300)
- Scannapieco, E. & Oh, S. P. 2004, *ApJ*, 608, 62
- Schirber, M., Miralda-Escudé, J., & McDonald, P. 2004, *ApJ*, 610, 105
- Schlegel, D. J., Finkbeiner, D. P., & Davis, M. 1998, *ApJ*, 500, 525
- Schlegel, D. J., et al. 2005 in preparation
- Schneider, D. P., Schmidt, M., & Gunn, J. E. 1994, *AJ*, 107, 1245
- Schneider, D. P., et al. 2000, *AJ*, 120, 2183
- Schneider, D. P., et al. 2005, *AJ*, in press (astro-ph/0503679)
- Schneider, P. 1993, *Gravitational Lenses in the Universe*, 41
- Sembach, K. R. & Savage, B. D. 1992, *ApJS*, 83, 147
- Serber, W., et al. 2004 in preparation
- Shanks, T. & Boyle, B. J. 1994, *MNRAS*, 271, 753
- Shaver, P. A. 1984, *A&A*, 136, L9
- Sheldon, E. S., et al. 2004, *AJ*, 127, 2544
- Small, T. A., Sargent, W. L. W., & Steidel, C. C. 1997, *AJ*, 114, 2254
- Small, T. A. & Blandford, R. D. 1992, *MNRAS*, 259, 725
- Smith, J. A., et al. 2002, *AJ*, 123, 2121
- Smith, R. J., Boyle, B. J., & Maddox, S. J. 1995, *MNRAS*, 277, 270
- Smith, R. J., Boyle, B. J., & Maddox, S. J. 2000, *MNRAS*, 313, 252
- Spergel, D. N., et al. 2003, *ApJS*, 148, 175
- Sramek, R. A., & Weedman, D. W. 1978, *ApJ*, 221, 468
- Steidel, C. C., & Sargent, W. L. W. 1991, *AJ*, 102, 1610
- Stephens, A. W., Schneider, D. P., Schmidt, M., Gunn, J. E., & Weinberg, D. H. 1997, *AJ*, 114, 41
- Stiavelli, M., et al. 2005, *ApJ*, 622, L1
- Stoughton, C., et al. 2002, *AJ*, 123, 485
- Strauss, M. A., et al. 2002, *AJ*, 124, 1810
- Subramanian, K., Rees, M. J., & Chitre, S. M. 1987, *MNRAS*, 224, 283
- Teplitz, H. I., McLean, I. S., & Malkan, M. A. 1999, *ApJ*, 520, 469
- Toomre, A. & Toomre, J. 1972, *ApJ*, 178, 623
- Tremaine, S., et al. 2002, *ApJ*, 574, 740
- Turner, E. L. 1991, *AJ*, 101, 5
- Turner, E. L., Goldberg, R. E., & Gunn, J. E. 1982, *BAAS*, 14, 974
- Turner, E. L., et al. 1986, *Nature*, 321, 142
- Turner, E. L., Hillenbrand, L. A., Schneider, D. P., Hewitt, J. N., & Burke, B. F. 1988, *AJ*, 96, 1682
- Vanden Berk, D. E., et al. 2001, *AJ*, 122, 549
- Vanden Berk, D. E., et al. 2005, *ArXiv Astrophysics e-prints*, astro-ph/0501113
- Vilenkin, A. 1984, *ApJ*, 282, L51
- Wake, D. A., et al. 2004, *ApJ*, 610, L85
- Walsh, D., Carswell, R. F., & Weymann, R. J. 1979, *Nature*, 279, 381
- Weedman, D. W., Weymann, R. J., Green, R. F., & Heckman, T. M. 1982, *ApJ*, 255, L5
- Weinstein, M. A., et al. 2004, *ApJS*, 155, 243
- Wold, M., Lacy, M., Lilje, P. B., & Serjeant, S. 2001, *MNRAS*, 323, 231
- Wyithe, J. S. B. & Loeb, A. 2002a, *ApJ*, 577, 57
- Wyithe, J. S. B. & Loeb, A. 2002b, *ApJ*, 581, 886
- Wyithe, S. & Loeb, A. 2004, *ArXiv Astrophysics e-prints*, astro-ph/0403714
- Yee, H. K. C. & Green, R. F. 1984, *ApJ*, 280, 79
- Yee, H. K. C. & Green, R. F. 1987, *ApJ*, 319, 28
- York, D. G., et al. 2000, *AJ*, 120, 1579
- Yu, Q. & Tremaine, S. 2002, *MNRAS*, 335, 965
- Zehavi, I., et al. 2004, *ApJ*, 608, 16
- Zehavi, I., et al. 2005, *ApJ*, 621, 22
- Zhdanov, V. I. & Surdej, J. 2001, *A&A*, 372, 1